

# Topology Optimization under Uncertainty using a Stochastic Gradient-based Approach

Subhayan De · Jerrad Hampton · Kurt Maute · Alireza Doostan

Received: date / Accepted: date

**Abstract** Topology optimization under uncertainty (TOuU) often defines objectives and constraints by statistical moments of geometric and physical quantities of interest. Most traditional TOuU methods use gradient-based optimization algorithms and rely on accurate estimates of the statistical moments and their gradients, *e.g.*, via adjoint calculations. When the number of uncertain inputs is large or the quantities of interest exhibit large variability, a large number of adjoint (and/or forward) solves may be required to ensure the accuracy of these gradients. The optimization procedure itself often requires a large number of iterations, which may render the TOuU problem computationally expensive, if not infeasible, due to the overall large number of required adjoint (and/or forward) solves. To tackle this difficulty, we here propose an optimization approach that generates a stochastic approximation of the objective, constraints, and their gradients via a small number of adjoint (and/or forward) solves, per optimization iteration. A statistically independent (stochastic) approximation of these quantities is generated at each optimization iteration. This approach results in a total cost that is a small factor larger than that of the corresponding deterministic TO problem. We incorporate the stochastic approximation of objective, constraints and their design sensitivities into two classes of optimization algorithms. First, we investigate the stochastic gradient descent (SGD) method and a number of its variants, which have been successfully applied to large-scale optimization problems for machine learning. Second, we study the use of stochastic approximation approach within conventional nonlinear programming methods, focusing on the Globally Convergent Method of Moving Asymptotes (GCMMA), a widely utilized scheme in de-

---

S. De  
Smead Aerospace Engineering Sciences Department, University of Colorado, Boulder, CO 80309, USA  
E-mail: Subhayan.De@colorado.edu

J. Hampton  
E-mail: Jerrad.Hampton@colorado.edu  
· K. Maute  
E-mail: Kurt.Maute@colorado.edu  
· A. Doostan (✉)  
E-mail: Alireza.Doostan@colorado.edu

terministic TO. The performance of these algorithms is investigated with structural design problems utilizing Solid Isotropic Material with Penalization (SIMP) based optimization, as well as an explicit level set method. These investigations, conducted on both two- and three-dimensional structures, illustrate the efficacy of the proposed stochastic gradient approach for TOuU applications.

## 1 Introduction

Finding the optimum geometry and arrangement of materials for the design of engineered materials and components are key challenges across many applications. These challenges become even more complicated in the presence of uncertainty resulting from, *e.g.*, manufacturing imprecision or incomplete/inaccurate measurements. In structural topology optimization (TO) (Sigmund and Petersson, 1998; Sigmund and Maute, 2013), the arrangement of one or multiple materials within a design domain is investigated to optimize the mechanical performance of a structure while accounting for design constraints. In recent years, TO has been used in several other fields, such as fluid flows, acoustics, optics, and multi-physics applications. The reader is referred to the survey papers by Sigmund and Maute (2013); Deaton and Grandhi (2014).

In the presence of uncertainty, we often seek *robust* designs that provide a compromise between mean performance and insensitivity to variation in geometry, material properties, such as elastic modulus or heat conductivity of the material, and operating conditions. A poor understanding of uncertainties in these system inputs can lead to poor design choices (Schuëller and Jensen, 2008). In this paper, we consider TO problems with uncertainties in geometry, loading conditions, and material properties, which we model as random variables. We refer to this TO in the presence of uncertainty as topology optimization under uncertainty (TOuU), similar to Conti et al. (2009); Tootkaboni et al. (2012); Maute (2014); Keshavarzzadeh et al. (2017).

The effects of uncertainty in TO were first considered by adding a probabilistic constraint mostly based on the probability of failure (Bae and Wang, 2002; Maute and Frangopol, 2003; Kharmanda et al., 2004; Jung and Cho, 2004; Moon et al., 2004; Kim et al., 2006; Mogami et al., 2006; Eom et al., 2011). This approach is known as reliability-based topology optimization (RBTO) and mostly uses first-order or second-order Taylor series expansion for performance function (Haldar and Mahadevan, 2000). On the other hand, Eldred and Elman (2011) and Keshavarzzadeh et al. (2016) used polynomial chaos expansion method (Ghanem and Spanos, 2003) to solve RBTO. In these studies, the uncertainty is assumed to be present in the loads, in the material properties, such as the modulus of elasticity and yield stress, or in the thickness of the structural components.

Robust TO, on the other hand, considers the effects of uncertainty in the objective and constraints through higher order statistics, *e.g.*, variance. Alvarez and Carrasco (2005), Dunning et al. (2011), and Dunning and Kim (2013) considered uncertainties in the loading magnitude and direction and minimized expected and/or variance of the compliance of the structure. Guest and Igusa (2008) also considered uncertainties in nodal locations of a truss and derived expressions for corresponding equivalent random forces for the minimization of expected compliance. TO under geometric un-

certainty has also been investigated in [Chen et al. \(2010\)](#) and [Chen and Chen \(2011\)](#). These authors used a Karhunen-Loeve expansion to represent the random field resulting from material, geometry and loading uncertainties. Perturbations in stiffness matrix are used in [Asadpoure et al. \(2011\)](#), [Zhao and Wang \(2014\)](#), and [Jansen et al. \(2015\)](#) to estimate the statistical moments of the compliance by Monte Carlo approximations. [Tootkaboni et al. \(2012\)](#), [Lazarov et al. \(2012\)](#), [Keshavarzzadeh et al. \(2017\)](#), and [Zhang and Kang \(2017\)](#) used polynomial chaos expansions while considering uncertainties in the loading and geometry of the structure and estimated the mean and variance of the compliance. A combined reduced-order modeling and polynomial chaos expansion approach for shape optimization has been proposed in [Maute et al. \(2009\)](#).

Monte Carlo simulation approaches use a large number of gradient evaluations at independent samples of inputs to form sample average estimates of the gradients. The number of required evaluations is large when the variances of the gradients are large. This, in turn, will lead to a high computational cost. Taylor series based perturbations are computationally efficient; however, they lose accuracy when the objective and constraints depend on the input uncertainties in a highly nonlinear manner. While methods based on polynomial chaos expansion are frequently used, they suffer from the *curse of dimensionality*, *i.e.*, the number of expansion coefficients increases rapidly with the number of uncertain parameters. Sparse polynomial chaos expansions ([Doostan et al., 2009](#); [Doostan and Owhadi, 2011](#); [Blatman and Sudret, 2010](#); [Hampton and Doostan, 2016](#)) can be used to reduce the computational cost, but for problems with a large number of uncertain inputs, such as TO with multiple uncertainty sources, the computational cost associated with this approach also becomes unbearable.

To alleviate the computational burden and motivated by the recent progress in stochastic gradient descent (SGD) methods, ([Bottou et al., 2018](#)), we advocate for a new approach for ToUU that uses a stochastic approximation of the gradients. In detail, we generate an unbiased, approximation of the gradients in a manner similar to the standard Monte Carlo approach but with a small, *e.g.*, 4 or 10, number of Monte Carlo samples of the gradient. Unlike in the standard Monte Carlo approach, we generate statistically independent estimates of the gradient in each optimization iteration. The small sample size gradient estimates are essentially stochastic approximations of those computed via standard Monte Carlo approach, hence the term *stochastic gradients*. Using these stochastic gradients, as we will illustrate in Section 2.4, the ToUU problem may be solved successfully via gradient descent methods that have recently seen significant use for high-dimensional problems arising in machine learning ([Bottou, 2010, 2012](#); [Sutskever et al., 2013](#)).

Recently, [Martin et al. \(2018\)](#) analyzed standard SGD method with variable step size to solve an optimal control problem, where the underlying partial-differential equation is solved using the finite element method and used as a constraint. When compared to the standard Monte Carlo method with fixed random samples, [Martin et al. \(2018\)](#) showed that the use of SGD can improve the computational cost by a logarithmic factor. In contrast to these investigations, in the present study, we consider the use of improved variants of SGD for non-convex TO problems, and to our best knowledge, this is the first such investigation. We explore AdaGrad ([Duchi et al.,](#)

2011) and Adam (Kingma and Ba, 2014), which are variants of the SGD method that retard the movement in directions with historically large gradient magnitudes, being useful for problems that lack convexity. To a lesser extent, we investigate methods like Stochastic Average Gradient (SAG) (Roux et al., 2012), which performs well on objectives that are strongly-convex, stochastic variance reduced gradient (SVRG) (Johnson and Zhang, 2013), and Adadelta (Zeiler, 2012). Second, we study the performance of a standard nonlinear programming method when supplying stochastic gradients. We focus on the Globally Convergent Method of Moving Assymptotes (GCMMA) by Svanberg (1987), owing to its popularity for TO. However, with GCMMA we need to provide objective and constraint information in addition to gradients contrary to the SGD methods.

In this paper, we describe the geometry and material distribution by either an explicit level set method or by a combination of level set and density-based approaches. The explicit level set method follows the work of Kreissl and Maute (2012), Villanueva and Maute (2014), and Sharma et al. (2017). For the density approach, we build on the Solid Isotropic Material with Penalization (SIMP) method (Bendsøe, 1989; Zhou and Rozvany, 1991; Sigmund and Maute, 2013). We illustrate the use of stochastic gradients in SGD methods and the GCMMA with two static linear elastic problems. Uncertainty in geometry, material properties, and loading conditions is considered. The results show that Adam and GCMMA supplied with stochastic gradients produce designs that are robust in presence of uncertainty. Further, only a handful of random samples are needed at every iteration, thus reducing the cost of TOuU to a small factor of the cost of deterministic TO.

The rest of the paper is organized as follows. Section 2 gives a brief background on the TO approaches used in this paper and provides a short outline on different SGD methods in practice and GCMMA. Then, we formulate the TOuU problem. In Section 3, we illustrate the performance of the stochastic gradient-based methods with two TO problems under uncertainty. Finally, in Section 4, we conclude the paper with a discussion on our observations.

## 2 Methodology

### 2.1 Design Model

In this paper, we describe the geometry and material layout within a specified design domain by an explicit level set method. The parameters of the discretized level set functions are defined explicitly in terms of the optimization variables. To this end, we follow closely the work of Kreissl and Maute (2012); Villanueva and Maute (2014). To mitigate the dependence of the optimization results on the initial level set function and to bypass the need of introducing additional techniques for seeding inclusions and holes, such as topological derivatives, we combine the explicit level set function with a density approach, namely the SIMP method.

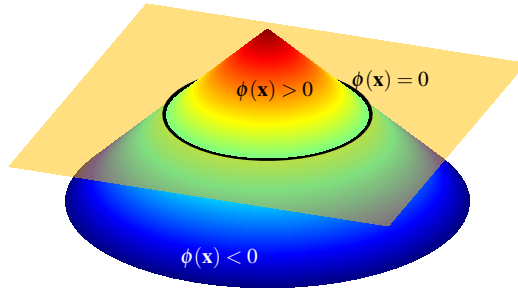
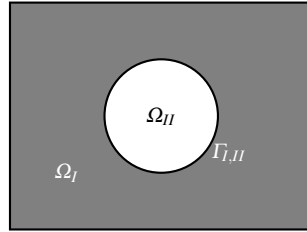
(a) Level set field  $\phi(\mathbf{x})$ .(b) Subdomains  $\Omega_I$  and  $\Omega_{II}$  with interface  $\Gamma_{I,II}$ .

Fig. 1: An example of level set field  $\phi(\mathbf{x})$  with corresponding subdomains  $\Omega_I$  and  $\Omega_{II}$ , and interface  $\Gamma_{I,II}$ .

Considering a two-phase problem, the level set field  $\phi(\mathbf{x})$  decomposes the design domain  $\Omega_D$  into two distinct subdomains  $\Omega_I$  and  $\Omega_{II}$  as follows:

$$\mathbf{x} \in \begin{cases} \Omega_I \forall \phi(\mathbf{x}) < 0; \\ \Omega_{II} \forall \phi(\mathbf{x}) > 0; \\ \Gamma_{I,II} \forall \phi(\mathbf{x}) = 0, \end{cases} \quad (1)$$

where  $\mathbf{x}$  denotes the spatial coordinates and  $\Gamma_{I,II}$  the interface between  $\Omega_I$  and  $\Omega_{II}$  as shown in Figure 1. In this paper, the level set function,  $\phi(\mathbf{x})$  is discretized by bi-linear and tri-linear shape functions in 2D and 3D, respectively. The nodal level set values,  $\phi_i$ , are defined as functions of the optimization and random variables.

To account specifically for shape imperfections, we consider structures made of an assembly of geometric primitives (Guo et al., 2014; Norato and Tortorelli, 2015; Zhang et al., 2016; Liu et al., 2018). Each primitive is defined by a small number of parameters that are treated as optimization and/or random variables. In this paper, we study examples where a 2D structure is composed of  $n_r$  rectangles or bars. The level set field associated with a single rectangle,  $\phi_r$ , is given in a local coordinate system,

$(\tilde{x}, \tilde{y})$ , as follows:

$$\phi_r = \left( \left( \frac{\tilde{x}}{a_r} \right)^\mu + \left( \frac{\tilde{y}}{b_r} \right)^\mu \right)^{1/\mu} - 1, \quad (2)$$

where the parameters  $a_r$  and  $b_r$  denote the dimensions of the rectangle, and  $\mu$  controls the sharpness of its corners. Note that the value of the level set function within the rectangle is negative. The local and the global coordinates are related by the following coordinate transformation:

$$\begin{bmatrix} \tilde{x} \\ \tilde{y} \end{bmatrix} = \begin{bmatrix} \cos(\alpha_r) & \sin(\alpha_r) \\ -\sin(\alpha_r) & \cos(\alpha_r) \end{bmatrix} \begin{bmatrix} x - x_r^c \\ y - y_r^c \end{bmatrix}, \quad (3)$$

where the center for the rectangle is defined by  $(x_r^c, y_r^c)$  and  $\alpha_r$  denotes the angle between the coordinate axes. The assembly of bars within the design domain is defined by the minimum of all level set values  $\phi_r$  at a point  $\mathbf{x}$ . To obtain a differentiable function  $\phi(\mathbf{x})$  we approximate the minimum level set value at Node  $i$  by the Kreisselmeier-Steinhauser function:

$$\phi_i = \frac{1}{\beta_{KS}} \ln \left( \sum_{r=1}^{n_r} e^{\beta_{KS} \phi_r(\mathbf{x}_i)} \right) \quad \beta_{KS} < 0, \quad (4)$$

where  $\mathbf{x}_i$  are the coordinates at Node  $i$ , and the parameter  $\beta_{KS}$  controls the accuracy of the approximation. Assuming that all bars are made of a single material, the geometry of the structure is defined by the  $n_r$  set of the following five parameters:  $\{a_r, b_r, x_r^c, y_r^c, \alpha_r\}$ . These parameters will be treated as design and random parameters in the numerical examples of Section 3.1.

To increase the design freedom over the geometric primitive approach, we assign each node  $i$ ,  $i = 1, \dots, n_N$ , in the mesh an optimization variable  $\theta_i$  and define the level set values at Node  $j$  as follows:

$$\phi_j = \phi_s (\phi_t - \tilde{\theta}_j) \quad \text{with} \quad 0 \leq \tilde{\theta}_j \leq 1; \quad j = 1 \dots n_N, \quad (5)$$

where the parameter  $\phi_s$  scales the level set field and the parameter  $\phi_t$  allows shifting the zero level set value with respect to the smoothed optimization variable  $\tilde{\theta}$ . The scaling parameter  $\phi_s$  is typically set relative to the element size  $h_e$ , e.g.,  $\phi_s = 3.0 h_e$ . The smoothed optimization variable  $\tilde{\theta}$  is defined by the linear filter:

$$\tilde{\theta}_j = \frac{\sum_{i=1}^{n_N} w_{ij} \theta_i}{\sum_{i=1}^{n_N} w_{ij}} \quad \text{with} \quad w_{ij} = \max(0, r_f - |\mathbf{x}_i - \mathbf{x}_j|); \quad 0 \leq \theta_i \leq 1; \quad i = 1 \dots n_N, \quad (6)$$

where  $r_f$  is a filter radius. Previous studies (Kreissl and Maute, 2012) suggested that the linear filter (6) promotes smooth boundaries and accelerates convergence as it increases the zone of influence of an optimization variable.

Traditional level set methods are exclusively driven by shape sensitivities and advance the geometry in the optimization process only along external boundaries and interfaces. This feature may lead to a noticeable dependency of the optimization results on the initial level set function. Furthermore, additional information is

required to seed new inclusions and holes. Topological derivatives (Novotny et al., 2003; Burger et al., 2004; Novotny et al., 2007) have been proposed to identify locations to seed new holes at distinct optimization steps, leading to discontinuities in the optimization process. To mitigate these discontinuities and as topological derivatives assume an infinitesimal hole, the size of the hole to be inserted into the discretized model should be as small as possible. However, evolving small holes into their final shape may require a large number of optimization steps.

In the present work, we combine density and level set methods to reduce the dependence of optimization results on the initial design and to mitigate the need for additional inclusion and hole seeding techniques. The density method is used first to determine the conceptual layout of the structure, and then the level set method is used to find the detailed geometry. To facilitate the smooth transition from the density to the level set method, we define the following SIMP model:

$$\begin{aligned}\theta_e &= \theta_s + \frac{1 - \theta_s}{n_E} \sum_{k=1}^{n_E} \tilde{\theta}_k, \\ \rho_e &= \rho_0 \theta_e, \\ E_e &= E_0 \theta_e^{\beta_{\text{SIMP}}},\end{aligned}\tag{7}$$

where  $\theta_e$  is an auxiliary elemental variable that depends on the average nodal variables  $\tilde{\theta}_k$  and a shift parameter  $\theta_s$ ,  $0 \leq \theta_s \leq 1$ . The number of nodes per element is  $n_E$ . The element-wise constant material density,  $\rho_e$ , and Young's modulus,  $E_e$ , are defined by a standard SIMP model. The bulk properties are denoted by  $\rho_0$  and  $E_0$ , and the SIMP penalty parameter is  $\beta_{\text{SIMP}}$ .

To perform standard SIMP TO, we set the level set shift parameters to  $\phi_l = -\varepsilon$ ,  $0 < \varepsilon \ll 1$  such that the level set values are strictly negative in the entire design domain, *i.e.*,  $\Omega_D = \Omega_l$ . To perform level set TO with a uniform bulk material, we set  $\phi_l = 0.5$  and the density shift parameter to  $\theta_s = 1.0$ . Note that other parameter values also allow optimizing simultaneously the material properties and the geometry defined by the phase boundary  $\Gamma_{l,l}$ , *i.e.*, the zero level set iso-contour. This option is not considered in the present work, however.

## 2.2 Analysis Model

This study considers structural optimization problems where the physical response is described by a static linear elastic model. Following the work of (Villanueva and Maute, 2014; Sharma et al., 2017), we discretize the governing equations by the eXtended Finite Element Method (XFEM). A generalized Heaviside enrichment strategy is used to consistently approximate the displacement field in the solid domain  $\Omega_l$  with  $\Omega_{ll}$  being void. To mitigate ill-conditioning caused by particular intersection configurations, we stabilize the XFEM formulation by the face-oriented Ghost Penalty Method (Burman and Hansbo, 2014; Schott et al., 2014).

For a specific realization of the design and boundary conditions, we compute the design sensitivities, *i.e.*, the gradients of the objective and gradients measures by the adjoint method. Details of evaluating the sensitivities using the adjoint method

can be found in [Sharma et al. \(2017\)](#). Depending on the optimization algorithm, these gradients are used directly or modified to determine the search direction in the optimization process. Details for the optimization algorithms considered in this study are presented in the next subsection.

### 2.3 Topology Optimization under Uncertainty (TOuU) Problem Formulation

Let  $\boldsymbol{\theta} \in \mathbb{R}^{n_\theta}$  denote the vector of optimization variables, and  $\boldsymbol{\xi} \in \mathbb{R}^{n_\xi}$  the vector of random variables associated with the problem. Let  $f(\boldsymbol{\theta}; \boldsymbol{\xi}) : \mathbb{R}^{n_\theta} \times \mathbb{R}^{n_\xi} \rightarrow \mathbb{R}$  denote the deterministic performance measure given  $\boldsymbol{\theta}$ , which also depends on the realized values of  $\boldsymbol{\xi}$ . Similarly, let  $\mathbf{g}(\boldsymbol{\theta}; \boldsymbol{\xi}) : \mathbb{R}^{n_\theta} \times \mathbb{R}^{n_\xi} \rightarrow \mathbb{R}^{n_g}$  be  $n_g$  real-valued deterministic measure of the constraints, which potentially depend on realized values of  $\boldsymbol{\xi}$ . We say that  $\boldsymbol{\theta}$  satisfies the constraints if  $\mathbf{g}(\boldsymbol{\theta}; \boldsymbol{\xi}) \leq 0$  and refer to any positive value of  $\mathbf{g}(\boldsymbol{\theta}; \boldsymbol{\xi})$  as a constraint violation of that magnitude. In structural TO, the function  $f$  is often the strain energy density and the constraint functions,  $\mathbf{g}$ , often include the volume or mass of the structure.

In the present study, for TOuU, we use objective as combination of its expected value and variance as follows

$$R(\boldsymbol{\theta}) = \mathbb{E}[f(\boldsymbol{\theta}; \boldsymbol{\xi})] + \lambda \text{Var}(f(\boldsymbol{\theta}; \boldsymbol{\xi})), \quad (8)$$

where  $\mathbb{E}[\cdot]$  and  $\text{Var}(\cdot)$  denote the mathematical expectation and variance of their arguments, respectively. Similarly, the constraint function can also be expressed as

$$\mathbf{C}_j(\boldsymbol{\theta}) = \mathbb{E}[\mathbf{g}_j(\boldsymbol{\theta}; \boldsymbol{\xi})] + \lambda \text{Var}(\mathbf{g}_j(\boldsymbol{\theta}; \boldsymbol{\xi})), \quad j = 1, \dots, n_g. \quad (9)$$

We note that while  $f$  and  $\mathbf{g}$  are random variables and random vector, respectively,  $R$  and  $\mathbf{C}$  are not as they are associated with moments taken with respect to the probability measure of  $\boldsymbol{\xi}$ . Here, the parameter  $\lambda \geq 0$  denotes the importance of variations in  $f$  or  $\mathbf{g}$ , relative to their means. The effect of adding the variance to the objective is to produce a design that shows little variations in the two responses, namely,  $f$  and  $\mathbf{g}$  even in the presence of uncertainty. Hence, we denote this formulation as *robust optimization* formulation for  $\lambda > 0$ . Although one may use different values of  $\lambda$  in (8) and (9) here we restrict our investigation to utilizing the same  $\lambda$  for both functions. Therefore, we are interested here in solving a problem of the type,

$$\min_{\boldsymbol{\theta}} R(\boldsymbol{\theta}) \text{ subject to } \mathbf{C}(\boldsymbol{\theta}) \leq \mathbf{0}, \quad (10)$$

or the closely related unconstrained formulation,

$$\min_{\boldsymbol{\theta}} R(\boldsymbol{\theta}) + \boldsymbol{\kappa}^T \mathbf{G}(\mathbf{C}(\boldsymbol{\theta})), \quad (11)$$

where  $\mathbf{G}_i(\mathbf{C}(\boldsymbol{\theta})) = \max(0, \mathbf{C}_i(\boldsymbol{\theta}))$ . In (11),  $\boldsymbol{\kappa}$  is a user-specified hyperparameter that weighs the importance of the constraints relative to the objective, achieving a balance between minimizing the objective function and the constraint functions. However, for TO, an extensive search for  $\boldsymbol{\kappa}$  is not computationally feasible. Hence, based on a few preliminary runs the values of  $\boldsymbol{\kappa}$  are decided in the numerical examples of this paper.



In standard Monte Carlo approach, we approximate  $R(\boldsymbol{\theta})$  and  $\mathbf{C}(\boldsymbol{\theta})$ , from (8) and (9) utilizing  $N_s$  forward solves of the model for specific values of the design variables  $\boldsymbol{\theta}$  and  $N_s$  realizations of  $\boldsymbol{\xi}$ . However, evaluating the functions  $f(\boldsymbol{\theta}, \boldsymbol{\xi})$  and  $\mathbf{g}(\boldsymbol{\theta}, \boldsymbol{\xi})$  at each iteration  $N_s$  times may be computationally expensive for structures with many degrees of freedom. Herein, we propose to use  $n$  number of random samples to estimate (8) and (9) where  $n \ll N_s$  (e.g.,  $n = 4, 10$ , etc.). We use the hat notation to denote an estimate of a quantity, and define the following

$$\widehat{\mathbb{E}}[f(\boldsymbol{\theta})] := \frac{1}{n} \sum_{i=1}^n f(\boldsymbol{\theta}; \boldsymbol{\xi}_i); \quad (12)$$

$$\widehat{\mathbb{E}}[\mathbf{g}(\boldsymbol{\theta})] := \frac{1}{n} \sum_{i=1}^n \mathbf{g}(\boldsymbol{\theta}; \boldsymbol{\xi}_i); \quad (13)$$

$$\widehat{\text{Var}}(f(\boldsymbol{\theta})) := \frac{1}{n-1} \sum_{i=1}^n \left( f(\boldsymbol{\theta}; \boldsymbol{\xi}_i) - \widehat{\mathbb{E}}(f(\boldsymbol{\theta})) \right)^2; \quad (14)$$

$$\widehat{\text{Var}}(\mathbf{g}(\boldsymbol{\theta})) := \frac{1}{n-1} \sum_{i=1}^n \left( \mathbf{g}(\boldsymbol{\theta}; \boldsymbol{\xi}_i) - \widehat{\mathbb{E}}(\mathbf{g}(\boldsymbol{\theta})) \right)^2; \quad (15)$$

$$\widehat{R}(\boldsymbol{\theta}) = \widehat{\mathbb{E}}[f(\boldsymbol{\theta})] + \lambda \widehat{\text{Var}}(f(\boldsymbol{\theta})); \quad (16)$$

$$\widehat{\mathbf{C}}_j(\boldsymbol{\theta}) = \widehat{\mathbb{E}}[\mathbf{g}_j(\boldsymbol{\theta})] + \lambda \widehat{\text{Var}}(\mathbf{g}_j(\boldsymbol{\theta})); \quad j = 1, \dots, n_g. \quad (17)$$

For brevity, these definitions do not explicitly state the dependence on  $\boldsymbol{\xi}$ .

We then approximate the gradients of the objective and constraints with respect to the design parameters via gradients of (16) and (17), which are identified via chain rule to be

$$\widehat{\mathbb{E}}[\nabla f(\boldsymbol{\theta})] := \frac{1}{n} \sum_{i=1}^n \nabla f(\boldsymbol{\theta}; \boldsymbol{\xi}_i); \quad (18)$$

$$\widehat{\mathbb{E}}[\nabla \mathbf{g}(\boldsymbol{\theta})] := \frac{1}{n} \sum_{i=1}^n \nabla \mathbf{g}(\boldsymbol{\theta}; \boldsymbol{\xi}_i); \quad (19)$$

$$\widehat{\mathbb{E}}(f(\boldsymbol{\theta}) \nabla f(\boldsymbol{\theta})) := \frac{1}{n} \sum_{i=1}^n f(\boldsymbol{\theta}; \boldsymbol{\xi}_i) \nabla f(\boldsymbol{\theta}; \boldsymbol{\xi}_i); \quad (20)$$

$$\widehat{\mathbb{E}}[\mathbf{g}(\boldsymbol{\theta}) \nabla \mathbf{g}(\boldsymbol{\theta})] := \frac{1}{n} \sum_{i=1}^n \mathbf{g}(\boldsymbol{\theta}; \boldsymbol{\xi}_i) \nabla \mathbf{g}(\boldsymbol{\theta}; \boldsymbol{\xi}_i); \quad (21)$$

$$\widehat{\text{Var}}(\nabla f(\boldsymbol{\theta})) := \frac{2n \left[ \widehat{\mathbb{E}}[f(\boldsymbol{\theta}) \nabla f(\boldsymbol{\theta})] - \widehat{\mathbb{E}}[f(\boldsymbol{\theta})] \widehat{\mathbb{E}}[\nabla f(\boldsymbol{\theta})] \right]}{(n-1)}; \quad (22)$$

$$\widehat{\text{Var}}(\nabla \mathbf{g}(\boldsymbol{\theta})) := \frac{2n \left[ \widehat{\mathbb{E}}[\mathbf{g}(\boldsymbol{\theta}) \nabla \mathbf{g}(\boldsymbol{\theta})] - \widehat{\mathbb{E}}[\mathbf{g}(\boldsymbol{\theta})] \widehat{\mathbb{E}}[\nabla \mathbf{g}(\boldsymbol{\theta})] \right]}{(n-1)}; \quad (23)$$

$$\nabla \widehat{R}(\boldsymbol{\theta}) = \widehat{\mathbb{E}}[\nabla f(\boldsymbol{\theta}; \boldsymbol{\xi})] + \lambda \widehat{\text{Var}}(\nabla f(\boldsymbol{\theta}; \boldsymbol{\xi})); \quad (24)$$

$$\nabla \widehat{\mathbf{C}}_j(\boldsymbol{\theta}) = \widehat{\mathbb{E}}[\nabla \mathbf{g}_j(\boldsymbol{\theta}; \boldsymbol{\xi})] + \lambda \widehat{\text{Var}}(\nabla \mathbf{g}_j(\boldsymbol{\theta}; \boldsymbol{\xi})); \quad j = 1, \dots, n_g, \quad (25)$$

where the  $n/(n-1)$  terms are to normalize to ensure unbiasedness. Notice that (18)-(25) hold as expectation and differentiation are linear operators. We note that in this

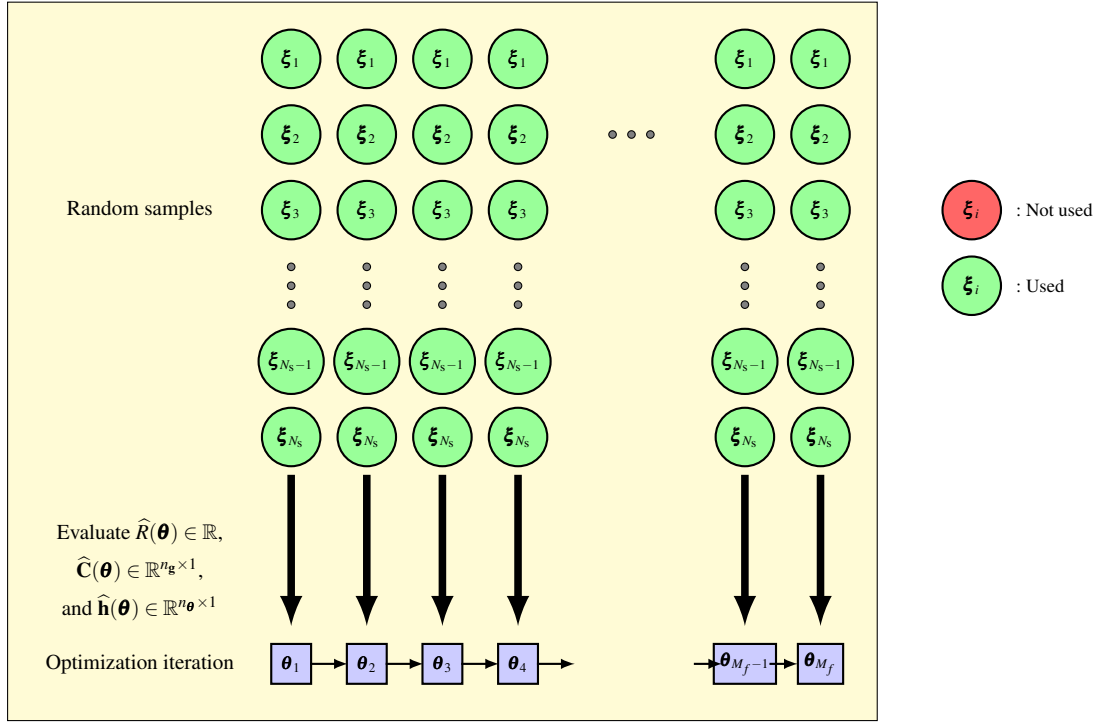
case, expectation and variance are computed coordinate-wise; specifically, there is no covariance information relying on correlations in different coordinates. Finally, the gradient for (11), which combines gradients of the objective and the constraint functions, is given by

$$\widehat{\mathbf{h}}(\boldsymbol{\theta}; \boldsymbol{\kappa}; \lambda) := \nabla \widehat{R}(\boldsymbol{\theta}) + \boldsymbol{\kappa}^T \widetilde{\nabla} \widehat{\mathbf{C}}(\boldsymbol{\theta}), \quad (26)$$

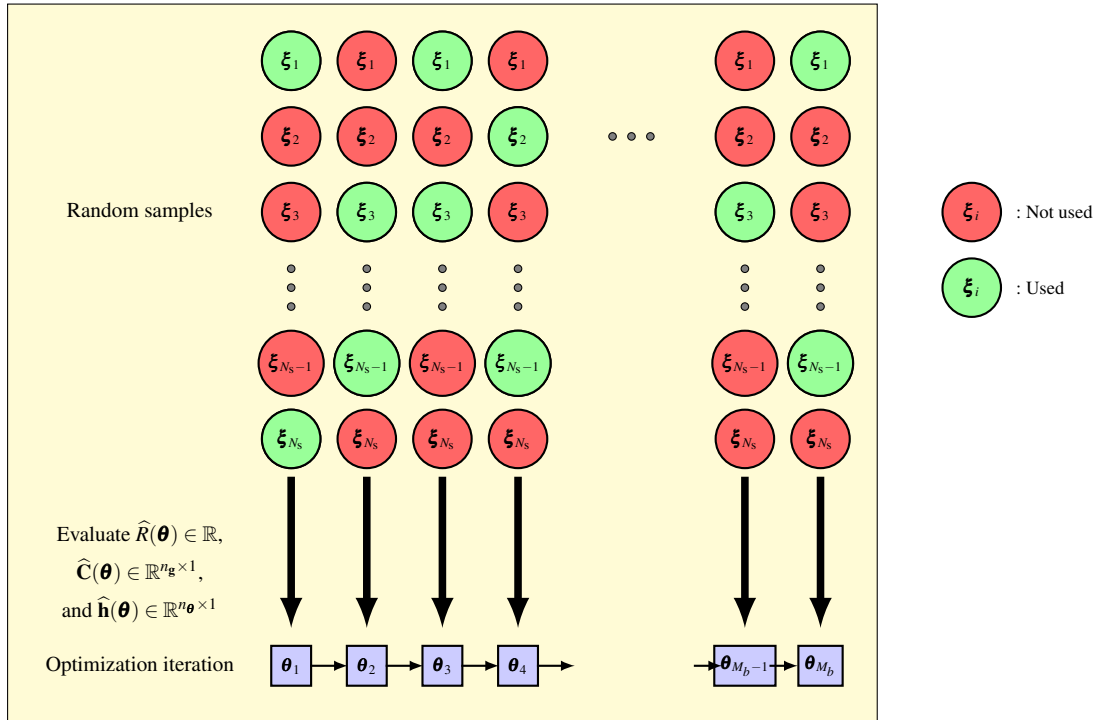
where  $\widetilde{\nabla} \widehat{\mathbf{C}}_j(\boldsymbol{\theta}) = \mathbf{0}$  if  $\widehat{\mathbf{C}}_j(\boldsymbol{\theta}) \leq 0$ ,  $j = 1, 2, \dots, n_g$ .

In this paper, the objective, constraints and their gradients are estimated at every design iteration with a small number of random samples  $\{\boldsymbol{\xi}_i\}_{i=1}^n$  instead of using all  $N_s$  samples with  $n \ll N_s$  resulting in a significant reduction in computational cost. These quantities thus calculated, however, are stochastic in nature. Hence, the gradients estimated in (24) and (25) using  $n$  random samples can be thought of as *stochastic gradients* calculated using a small batch of random samples (Ruder, 2016; Bottou et al., 2018). Note that, we compute only one mean gradient vector  $\widehat{\mathbf{h}}(\boldsymbol{\theta}; \boldsymbol{\kappa}; \lambda)$  at every iteration and not multiple mini-batches. Also, a single random sample  $\boldsymbol{\xi}$  can be used for mean design with variance weighting  $\lambda = 0$  but not with  $\lambda \neq 0$  as more than one sample is required to estimate the variance. For brevity, we suppress the dependence of  $\mathbf{h}$  on  $\boldsymbol{\kappa}$  and  $\lambda$ . However, to successfully implement the stochastic gradient methods for TOuU we need to use a different set of random samples for each iteration. The schematic of this approach is illustrated in Figure 2 and is compared with a standard Monte Carlo approach with full-batch gradients.

In this proposed approach, the samples in each mini-batch are statistically independent, so we analyze the samples in parallel, *i.e.*, we compute the objective and constraint measures as well as their gradients in parallel. The parallel implementation is straight forward and constitutes a trivial modification to (26). In the next two subsections, we discuss the SGD method, its variants, and GCMMA in brief, where we use these stochastic gradients.



(a) Schematic of the full-gradient approach



(b) Schematic of the proposed approach

Fig. 2: Comparison of the proposed approach for TOuU with a typical full-gradient approach utilizing  $N_s$  random samples for  $M_b$  and  $M_f$  optimization iterations, respectively. Note that, though total number of random samples  $N_s$  is finite in this schematic in reality it can be infinite.

## 2.4 Stochastic Gradient Descent (SGD) Method and its Variants

SGD method uses a single realization of  $\xi$  to update the design at the  $k$ th iteration utilizing the gradient  $\mathbf{h}_k$  (Bottou et al., 2018) that is defined by

$$\begin{aligned}\mathbf{h}_k &= \nabla f(\boldsymbol{\theta}_k, \xi_i) + \boldsymbol{\kappa}^T \widetilde{\nabla} \mathbf{g}(\boldsymbol{\theta}_k, \xi_i); \\ \boldsymbol{\theta}_{k+1} &= \boldsymbol{\theta}_k - \eta \mathbf{h}_k,\end{aligned}\tag{27}$$

where  $\eta$  is the step size, also known as the *learning rate*; and  $\widetilde{\nabla} \mathbf{g}_j(\boldsymbol{\theta}_k, \xi_i) = \mathbf{0}$  if  $\mathbf{g}_j(\boldsymbol{\theta}) \leq 0$ ,  $j = 1, 2, \dots, n_{\mathbf{g}}$ . Hence, the computational cost of stochastic gradient descent is very low. However, the convergence of the basic SGD method can be very slow since we might not follow the descent direction at every iteration. Instead, the descent is achieved in expectation as the expectation of the stochastic gradient is same as the gradient of the objective in (8). Note that, in literature, the use of a positive hyperparameter term  $\boldsymbol{\kappa}$  with SGD and its variants was mainly to introduce regularization (Tsuruoka et al., 2009; Lavergne et al., 2010; Collins and Kohli, 2014). In this study, we propose the use of  $\boldsymbol{\kappa}$  to enforce the design constraints.

A straightforward extension of the basic SGD method is to use a small batch of random samples to estimate the gradient  $\mathbf{h}_k$ . This version is known as *mini-batch gradient descent* (Ruder, 2016; Bottou et al., 2018) and will be further discussed in Section 2.3.

<b>Algorithm 1:</b> <i>Basic stochastic gradient descent method.</i> (Bottou et al., 2018)
--

<pre> Given <math>\eta</math>. Initialize <math>\boldsymbol{\theta}_1</math>. <b>for</b> <math>k = 1, 2, \dots</math> <b>do</b>     Compute <math>\mathbf{h}_k := \mathbf{h}(\boldsymbol{\theta}_k)</math>.     Set <math>\boldsymbol{\theta}_{k+1} \leftarrow \boldsymbol{\theta}_k - \eta \mathbf{h}_k</math>. [see Eqn. (27)] <b>end for</b> </pre>
--

In the past few years, different modifications to the above algorithm have been proposed to improve the convergence of SGD. Five such algorithms that we utilize here are presented next.

### 2.4.1 Adaptive Subgradient Methods (AdaGrad)

The first algorithm that we present is AdaGrad (Duchi et al., 2011), where historical information about the gradients is used to modify the update of optimization variables. It dampens the movements along directions with historically large gradients, thus adapting the learning rate and facilitating a faster convergence. In this algorithm, at iteration  $k$ , we compute the following auxiliary variable

$$\mathbf{a}_j = \sum_{i=1}^k \mathbf{h}_{i,j}^2, \quad j = 1, \dots, n_{\boldsymbol{\theta}},\tag{28}$$

which is then used in the following update rule

$$\boldsymbol{\theta}_{k+1} = \boldsymbol{\theta}_k - \eta \mathbf{a}^{-1/2} \mathbf{h}_k, \quad (29)$$

where the vector multiplication is performed component-wise. To avoid division by zero, a small number  $\varepsilon$  ( $= 10^{-8}$  used herein) is incorporated in the denominator of the update as shown in Algorithm 2.

**Algorithm 2: AdaGrad (Duchi et al., 2011)**

```

Given  $\eta$ .
Initialize  $\boldsymbol{\theta}_1$ .
Initialize  $\mathbf{a} := \mathbf{0}$ , having the same dimensions as  $\boldsymbol{\theta}_1$ .
for  $k = 1, 2, \dots$ , do
  Compute  $\mathbf{h}_k := \mathbf{h}(\boldsymbol{\theta}_k)$ .
  Set  $\mathbf{a}_j := \mathbf{a}_j + \mathbf{h}_{k,j}^2$ ,  $j = 1, \dots, n_{\boldsymbol{\theta}}$ .
  Set  $\boldsymbol{\theta}_{k+1,j} \leftarrow \boldsymbol{\theta}_{k,j} - \eta \frac{\mathbf{h}(\boldsymbol{\theta}_{k,j})}{\sqrt{\mathbf{a}_j + \varepsilon}}$ ,  $j = 1, \dots, n_p$ . [see Eqn. (29)]
end for

```

#### 2.4.2 Adadelta

The second algorithm that we study in this paper is Adadelta (Zeiler, 2012), which is similar to AdaGrad but reduces the window of historical gradients using an exponential decay rate  $\zeta$ , *i.e.*, at the  $k$ th iteration the gradient accumulation is estimated using

$$\mathbf{a}_{\mathbf{h},j} = \zeta \mathbf{h}_{k-1,j}^2 + (1 - \zeta) \mathbf{h}_{k,j}^2, \quad j = 1, \dots, n_{\boldsymbol{\theta}}. \quad (30)$$

Zeiler (2012) suggested a value of 0.95 for  $\zeta$  that we use here as well. A root-mean-square (RMS) of the gradient history accumulator is then defined as

$$\text{RMS}[\mathbf{h}_{k,j}] = \sqrt{\mathbf{a}_{\mathbf{h},j} + \varepsilon}. \quad (31)$$

Again, a very small number  $\varepsilon$  ( $= 10^{-8}$  used herein) is used to avoid division by zero. To be consistent with the units an accumulation of parameter update history is used,

$$\mathbf{a}_{\boldsymbol{\theta},j} = \zeta \mathbf{a}_{\boldsymbol{\theta},j} + (1 - \zeta) \Delta \boldsymbol{\theta}_{k,j}^2, \quad j = 1, \dots, n_{\boldsymbol{\theta}}, \quad (32)$$

where  $\Delta \boldsymbol{\theta}_k$  is the update of the parameter vector  $\boldsymbol{\theta}$  at iteration  $k$ . The RMS of the parameter update history becomes

$$\text{RMS}[\Delta \boldsymbol{\theta}_{k,j}] = \sqrt{\mathbf{a}_{\boldsymbol{\theta},j} + \varepsilon}. \quad (33)$$

The parameter update is then defined as

$$\begin{aligned} \Delta \boldsymbol{\theta}_k &= \frac{\text{RMS}[\Delta \boldsymbol{\theta}_k]}{\text{RMS}[\mathbf{h}_k]} \mathbf{h}_k, \\ \boldsymbol{\theta}_{k+1} &= \boldsymbol{\theta}_k - \Delta \boldsymbol{\theta}_k. \end{aligned} \quad (34)$$

The main steps of the Adadelta method are summarized in Algorithm 3. Note that, in this algorithm, we do not need the learning rate  $\eta$  explicitly.

**Algorithm 3: Adadelta (Zeiler, 2012)**

```

Given  $\rho, \varepsilon$ .
Initialize  $\boldsymbol{\theta}_1$ .
Initialize  $\mathbf{a}_h := \mathbf{0}$  and  $\mathbf{a}_\theta := \mathbf{0}$ , having the same dimensions as  $p_1$ .
for  $k = 1, 2, \dots$ , do
  Compute  $\mathbf{h}_k := \mathbf{h}(\boldsymbol{\theta}_k)$ .
  Set  $\mathbf{a}_{h,j} \leftarrow \zeta \mathbf{a}_{h,j} + (1 - \zeta) \mathbf{h}_{k,j}^2$ ,  $j = 1, \dots, n_\theta$ . [see Eqn. (30)]
  Evaluate  $\text{RMS}[\mathbf{h}_{k,j}] = \sqrt{\mathbf{a}_{h,j} + \varepsilon}$ ,  $j = 1, 2, \dots, n_\theta$ . [see Eqn. (31)]
  Evaluate  $\text{RMS}[\Delta \boldsymbol{\theta}_{k,j}] = \sqrt{\mathbf{a}_{\theta,k,j} + \varepsilon}$ ,  $j = 1, 2, \dots, n_\theta$ . [see Eqn. (33)]
  Set  $\Delta \boldsymbol{\theta}_{k,j} = \frac{\text{RMS}[\Delta \boldsymbol{\theta}_{k,j}]}{\text{RMS}[\mathbf{h}_{k,j}]} \mathbf{h}_{k,j}$ ,  $j = 1, 2, \dots, n_\theta$ .
  Set  $\boldsymbol{\theta}_{k+1,j} \leftarrow \boldsymbol{\theta}_{k,j} - \Delta \boldsymbol{\theta}_{k,j}$ ,  $j = 1, 2, \dots, n_\theta$ . [see Eqn. (34)]
  Set  $\mathbf{a}_{\theta,j} \leftarrow \zeta \mathbf{a}_{\theta,j} + (1 - \zeta) (\Delta \boldsymbol{\theta}_{k,j})^2$ ,  $j = 1, \dots, n_\theta$ . [see Eqn. (32)]
end for

```

**2.4.3 Adaptive Moment Estimation (Adam)**

Another algorithm that we consider in this paper for TO is Adam (Kingma and Ba, 2014). This algorithm is similar to Adagrad, but it intends to additionally smooth the variability in  $\mathbf{h}$  from iteration to iteration through the accumulation of historical gradient and squared gradient information. Two exponential decay rates  $\beta_m$  and  $\beta_v$  are used as follows

$$\begin{aligned} \mathbf{m}_k &= \beta_m \mathbf{m}_{k-1} + (1 - \beta_m) \mathbf{h}_k; \\ \mathbf{v}_{k,j} &= \beta_v \mathbf{v}_{k-1,j} + (1 - \beta_v) \mathbf{h}_{k,j}^2, \quad j = 1, 2, \dots, n_\theta. \end{aligned} \quad (35)$$

The authors of Adam (Kingma and Ba, 2014) recommend  $\beta_m = 0.9$  and  $\beta_v = 0.999$ , which we also use here. The following initialization bias correction is applied to the above-accumulated quantities

$$\begin{aligned} \hat{\mathbf{m}}_k &= \frac{\mathbf{m}_k}{1 - \beta_m^k}; \\ \hat{\mathbf{v}}_k &= \frac{\mathbf{v}_k}{1 - \beta_v^k}. \end{aligned} \quad (36)$$

Finally, the parameters are updated using

$$\boldsymbol{\theta}_{k+1,j} = \boldsymbol{\theta}_{k,j} - \eta \frac{\hat{\mathbf{m}}_j}{\sqrt{\hat{\mathbf{v}}_j} + \varepsilon} \quad j = 1, 2, \dots, n_\theta. \quad (37)$$

The main steps of the Adam algorithm are summarized in Algorithm 4.

**2.4.4 Stochastic Average Gradient (SAG)**

The next algorithm that we evaluate in this paper is the Stochastic Average Gradient or SAG (Roux et al., 2012), which updates the gradient information for one random

**Algorithm 4: Adam** (Kingma and Ba, 2014)

```

Given  $\eta$ ,  $\beta_m$ ,  $\beta_t$ , and  $\varepsilon$ .
Initialize  $\boldsymbol{\theta}_1$ .
Initialize  $\mathbf{m} = \mathbf{0}$ .
Initialize  $\mathbf{v} = \mathbf{0}$ .
for  $k = 1, 2, \dots$ , do
  Compute  $\mathbf{h}_k := \mathbf{h}(\boldsymbol{\theta}_k)$ .
  Set  $\mathbf{m} \leftarrow \beta_m \mathbf{m} + (1 - \beta_m) \mathbf{h}_k$ . [see Eqn. (35)]
  Set  $\mathbf{v}_j \leftarrow \beta_v \mathbf{v}_j + (1 - \beta_v) \mathbf{h}_{k,j}^2$   $j = 1, 2, \dots, n_{\boldsymbol{\theta}}$ . [see Eqn. (35)]
  Set  $\hat{\mathbf{m}} \leftarrow \mathbf{m} / (1 - \beta_m^k)$ . [see Eqn. (36)]
  Set  $\hat{\mathbf{v}} \leftarrow \mathbf{v} / (1 - \beta_v^k)$ . [see Eqn. (36)]
  Set  $\boldsymbol{\theta}_{k+1,j} \leftarrow \boldsymbol{\theta}_{k,j} - \eta \frac{\hat{m}_j}{\sqrt{\hat{v}_j + \varepsilon}}$   $j = 1, 2, \dots, n_{\boldsymbol{\theta}}$ . [see Eqn. (37)]
end for

```

sample at every iteration. The parameters are updated using

$$\boldsymbol{\theta}_{k+1} = \boldsymbol{\theta}_k - \frac{\eta}{N} \sum_{i=1}^{N_s} \mathbf{d}_{k,i}; \quad (38)$$

$$\mathbf{d}_{k,i} = \begin{cases} \mathbf{h}(\boldsymbol{\theta}_k; \boldsymbol{\xi}_i) & \text{if } i = t \in \{1, 2, \dots, N_s\}; \\ \mathbf{d}_{k-1,i} & \text{otherwise,} \end{cases}$$

where  $t$  is selected randomly from  $\{1, 2, \dots, N_s\}$ . This method minimizes a batch of  $N_s$  input uncertainty samples that is necessarily finite, as opposed to the typically infinite potential input uncertainties that are assumed by the random variable model.

**Algorithm 5: SAG** (Roux et al., 2012)

```

Given  $\eta$ .
Initialize  $\boldsymbol{\theta}_1$ .
Initialize  $\mathbf{d} = \mathbf{0}$ .
for  $k = 1, 2, \dots$ , do
  Draw  $t$  randomly from  $\{1, \dots, N_s\}$ .
  if  $i = t$  then
    Compute  $\mathbf{d}_i := \mathbf{h}(\boldsymbol{\theta}_k)$  for  $\boldsymbol{\xi}_t$ .
  end if
   $\boldsymbol{\theta}_{k+1} \leftarrow \boldsymbol{\theta}_k - \frac{\eta}{N_s} \sum_{i=1}^{N_s} \mathbf{d}_i$ . [see Eqn. (38)]
end for

```

#### 2.4.5 Stochastic Variance Reduced Gradient (SVRG)

The final algorithm that we consider in this work is the stochastic variance reduced gradient (SVRG) method (Johnson and Zhang, 2013). In this algorithm, a variance reduction method is introduced in SGD by maintaining a parameter estimate  $\boldsymbol{\theta}_{\text{best}}$  at every inner iteration that is updated only during the outer iterations. Using this

parameter estimate and the following estimate of the gradient

$$\mathbf{h}_{\text{best}} = \frac{1}{N_s} \sum_{i=1}^{N_s} \mathbf{h}(\boldsymbol{\theta}_{\text{best}}, \boldsymbol{\xi}_i), \quad (39)$$

an update rule similar to the SGD is applied. However, the gradient term is replaced with

$$\mathbf{h}(\boldsymbol{\theta}_k, \boldsymbol{\xi}_t) - \mathbf{h}(\boldsymbol{\theta}_{\text{best}}, \boldsymbol{\xi}_t) + \mathbf{h}_{\text{best}} \quad (40)$$

for randomly chosen  $t \in \{1, 2, \dots, N_s\}$  i.e.,  $\mathbf{h}(\boldsymbol{\theta}_{\text{best}})$  is used here as a control variate (Ross, 2013). These steps are illustrated in Algorithm 6.

**Algorithm 6: SVRG (Johnson and Zhang, 2013)**

```

Given  $\eta$  and  $m$ .
Initialize  $\tilde{\boldsymbol{\theta}}_1$ .
for  $j = 1, 2, \dots$ , do
  Set  $\boldsymbol{\theta}_{\text{best}} = \tilde{\boldsymbol{\theta}}_j$ .
  Set  $\mathbf{h}_{\text{best}} = \frac{1}{N_s} \sum_{i=1}^{N_s} \mathbf{h}(\boldsymbol{\theta}_{\text{best}}, \boldsymbol{\xi}_i)$ .
  Set  $\boldsymbol{\theta}_1 = \boldsymbol{\theta}_{\text{best}}$ .
  for  $k = 1, 2, \dots, m$  do
    Randomly choose  $t \in \{1, 2, \dots, N_s\}$ .
    Set  $\boldsymbol{\theta}_{k+1} \rightarrow \boldsymbol{\theta}_k - \eta [\mathbf{h}(\boldsymbol{\theta}_k, \boldsymbol{\xi}_t) - \mathbf{h}(\boldsymbol{\theta}_{\text{best}}, \boldsymbol{\xi}_t) + \mathbf{h}_{\text{best}}]$ . [see Eqn. (40)]
  end for
   $\tilde{\boldsymbol{\theta}}_j \leftarrow \boldsymbol{\theta}_{m+1}$  or  $\tilde{\boldsymbol{\theta}}_j \leftarrow \boldsymbol{\theta}_t$ , for randomly chosen  $t \in \{1, 2, \dots, m\}$ .
end for

```

We note that most of the SGD methods considered in this study depend on the learning rate parameter  $\eta$ , which controls the size of the step along the modified gradients. The tuning of this parameter is crucial to the success of these methods. For tuning, either a learning schedule can be followed or some pilot runs are needed. Since the overall cost of one iteration of the optimization is not significant given only a few samples are used at every iteration, these pilot runs do not add substantial cost to the overall optimization procedure. This aspect is further illustrated in Section 3.1. Note that a line search in the descent direction of the current iteration can also be performed removing the need for tuning of the learning rate parameter  $\eta$  (Mahsereci and Hennig, 2015); however, this is beyond the scope of the current paper.

## 2.5 Globally Convergent Method of Moving Asymptotes (GCMMA) with Stochastic Gradients

Owing to its popularity in TO, we also study the performance of globally convergent method of moving asymptotes (GCMMA) using stochastic gradients. In GCMMA, at every iteration, a convex subproblem is constructed using conservative approximations of the objective and constraint functions around the current optimization variable values. The solution of the subproblem is determined by solving its Karush-Kuhn-Tucker (KKT) conditions. GCMMA is well suited for large scale optimization



problems as the subproblem is separable, *i.e.*, it can be decomposed in  $n_\theta$  single-variable problems. In this paper, we supply GCMMA with stochastic gradients as outlined in the next section. Note that, in GCMMA we need to provide objective and constraint information as well. Hence, we perform forward solves in addition to estimating gradients using adjoint solves with only a few random samples per iteration for the numerical examples herein. This is in contrast to SGD methods, where only gradient information is needed at every iteration.

### 3 Numerical Examples

In this section, we investigate the characteristics and performance of using stochastic gradients with SGD methods and GCMMA for TOuU by two numerical examples. In both examples, we seek to minimize the expected compliance of the structures subject to a volume constraint. The structural response is described by a static linear elastic model. First, a 2D beam design problem is studied with the explicit level set approach of Section 2.1, using a primitive geometry parameterization of the design. We consider uncertainty in shape and topology. Second, we apply the combined density – level set method to a 3D problem with uncertainty in loading conditions and support stiffness. These examples have been chosen because they feature different influences of optimization variables and uncertain parameters on the objective and constraint. Since the TO problems considered here are non-convex, there may be several local minima. Therefore, different optimization algorithms may converge to different designs. To compare several algorithms in this work, we consider the value of the objective at the optimal solution to assess the performance of these methods, independently of the particular design obtained.

For both examples, each realization of a design candidate is analyzed by the XFEM using bi-linear elements in 2D and tri-linear elements in 3D. To suppress rigid body motion of structural members, we apply soft distributed fictitious springs to the solid domain; see Villanueva and Maute (2014). The gradients of the performance and constraint measures are computed by the adjoint method. The linear systems of the forward and sensitivity analyses are solved by a direct serial solver for the 2D problems and by an iterative parallel solver for the 3D problems. Further details of the XFEM formulation and sensitivity analysis used in these examples are outlined in Section 2.2. The algorithmic parameters controlling the behavior of the different optimization algorithms studied in the following are given with each example.

#### 3.1 Example I: Beam Design Problem

In this problem, we are interested in optimizing the geometry of a 2D structure that spans a gap, with a point load  $2P$  placed at the center of the gap on top of the structure. Design domain is formed by a  $6.0 \times 1.0$  rectangle. The structure is simply supported on the bottom left and right corners. By considering symmetry, we restrict our computational domain to one-half the size of the gap, where the load is placed at the top left corner, and the structure is supported at the bottom right corner; see Figure 3.

Bar parameter	Optimization Variable	Lower Bound	Upper Bound
$x_r^c$	$\theta_j$	0.0	3.0
$y_r^c$	$\theta_{j+1}$	0.0	1.0
$a_r$	$\theta_{j+2}$	0.0	3.15
$b_r$	$\theta_{j+3}$	0.0	0.1
$\alpha_r$	$\theta_{j+4}$	0.0	$\pi$

Table 1: Lower and upper bounds of bar parameters and optimization variables for  $r = 1 \dots 12$  and  $j = 5 (r - 1)$ .

The objective function of the optimization is the compliance of the system, and the constraint is to ensure the mass-ratio of the design area is no more than 15% of the maximum design mass (when entire design domain is filled with the material).

We describe the geometry of the structure by the explicit level set method with a geometric primitive parameterization of the level set function. We restrict the design space to structures that can be assembled with twelve rectangular bars in this half-domain. Each of these twelve bars is assumed to have five geometric parameters, which are allowed to vary; see Section 2.1. The total number of optimization variables is  $n_{\theta} = 60$ .

We introduce geometric uncertainties in this problem by assuming that the geometry parameters of the bars, *i.e.*,  $a_r, b_r, x_r^c, y_r^c, \alpha_r$ ,  $r = 1 \dots 12$ , are uncertain. We subject these parameters to uniform perturbations within 0.5% of their initial values as follows

$$\begin{aligned}
x_r^c &= \theta_j (1 + 0.005\xi_j); \\
y_r^c &= \theta_{j+1} (1 + 0.005\xi_{j+1}); \\
a_r &= \theta_{j+2} (1 + 0.005\xi_{j+2}); \quad \text{with } r = 1 \dots 12, j = 5 (r - 1) \\
b_r &= \theta_{j+3} (1 + 0.005\xi_{j+3}); \\
\alpha_r &= \theta_{j+4} (1 + 0.005\xi_{j+4});
\end{aligned} \tag{41}$$

where  $\xi_i$  is a uniform random variable on  $[-1, 1]$ . The lower and upper bounds of the optimization variables  $\theta_j$  are given in Table 1. If the perturbation of an optimization variable  $\theta_j$  by  $\xi_j$  would place the primitive bar outside of the shaded region in Figure 3 then that variable is replaced by the maximum or minimum allowed value. Hence, we set the bar parameters as

$$\begin{aligned}
x_r^c &= \max(0, \min(3, x_r^c)); \\
y_r^c &= \max(0, \min(1, y_r^c)); \\
a_r &= \max(0, \min(3.15, a_r)); \quad \text{with } r = 1 \dots 12. \\
b_r &= \max(0, \min(0.1, b_r)); \\
\alpha_r &= \max(0, \min(\pi, \alpha_r));
\end{aligned} \tag{42}$$

This uncertainty model mimics a scenario where, due to manufacturing imperfections, the built structure's dimensions may be slightly different from their designed values. Hence, in this example, the optimization and uncertainty parameters are closely connected. Note that, this problem is high-dimensional, *i.e.*,  $n_{\xi} = 60$ , and

methods based on PCE or sparse grids will not be efficient. We use Young's modulus  $E_0$ , the material density  $\rho_0$ , and the load as unity. The Poisson's ratio is assumed as 0.3. To avoid rigid body motion of disconnected material fictitious springs with spring constants  $10^{-6}$  are used. Finite elements with edge length 0.02 are used to solve the forward problem. We use  $\mu = 10$  in (2) to define the sharpness of the corners of the primitive rectangles and  $\beta_{KS} = -20$  in the Kreisselmeier-Steinhauser function (see (4)).

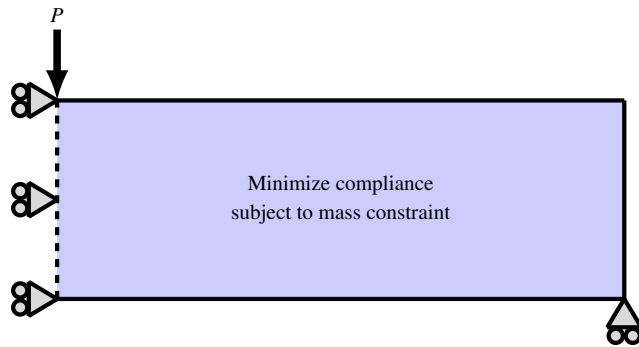
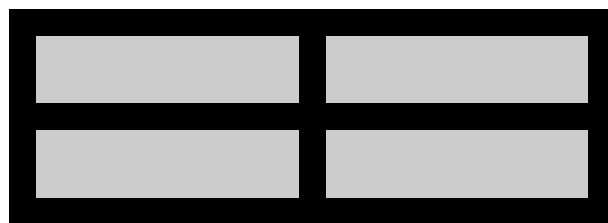


Fig. 3: Schematic for the beam design problem (design domain is shown as the shaded region).



(a) Initial structural design



(b) Final structural design

Fig. 4: Initial and final design for the beam design problem obtained using GCMMA in a deterministic setting.

This design problem is sensitive to the level of randomness in the geometry parameters and the desired robustness, *i.e.*, the weighting of the variance,  $\lambda$ , in the formulation of the objective (8). This sensitivity is primarily caused by the fact that due to small design changes and/or stochastic perturbations, either thin structural members disconnect or bars connect in an unfavorable fashion. Either case may lead to large changes in the objective function and dramatically reduced step sizes may be needed to obtain a stable convergence of the optimization process.

Here, we start with an initial design as shown in Figure 4. A final design obtained using GCMMA for this problem without the uncertainty is shown in Figure 4b. For this example, we have chosen  $\kappa = 700$  in (11), which is identified by preliminary numerical experimentations to be an appropriate level of  $\kappa$ .

### 3.1.1 Average Design

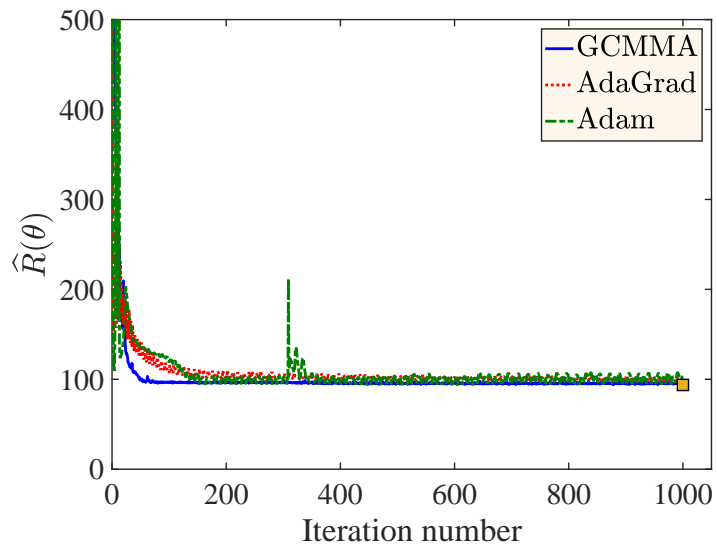
First, we consider solving the optimization problem (8) and (9), omitting the variance term in the objective, *i.e.*,  $\lambda = 0$ . We use a sample size of  $n = 4$  and learning rate  $\eta = 0.05$  for the algorithms in Section 2.3 (except for Adadelta). The learning rate is chosen based on some pilot runs.

To confine the presentation to the most relevant findings, we do not explicitly discuss results from methods that failed to converge and do not produce any meaningful designs, *e.g.*, the design shown in Figure 5. Specifically, the methods that are not shown in the legends of the plots in this paper have failed. These failures are the result of some designs having disconnected members which leads to poor designs with dramatically larger compliance. Similarly, we exclude methods that do not result in a converged solution with a significantly reduced objective.

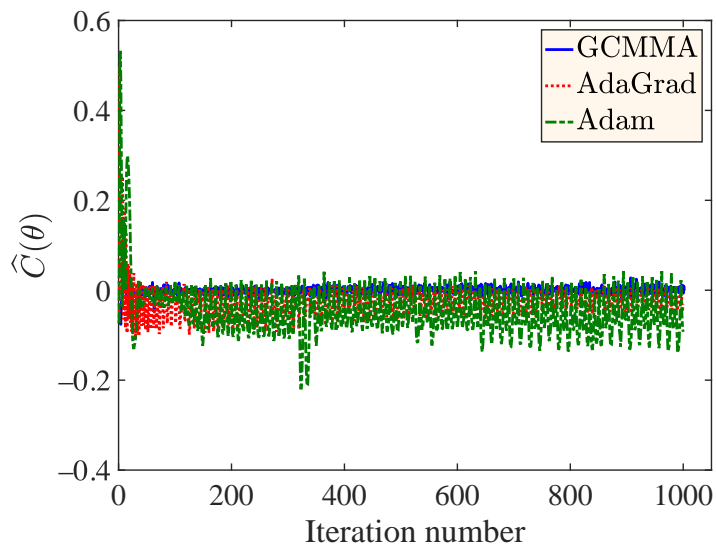


Fig. 5: An example of failed design obtained using SVRG with  $m = 10$  and  $\eta = 0.05$  (see Algorithm 6). Note that the two structural members are not connected; thus the compliance is infinite.

Figure 6 shows the mean objective and constraint values for designs constructed by the non-failing methods when using  $n = 4$  realizations of uncertain inputs at each iteration to form the estimates of the objective and constraint functions, as well as their gradients. Figure 6a shows that among the SGD methods, Adam outperforms AdaGrad. However, GCMMA supplied with stochastic gradients turns out to be the best among all the methods compared here. The optimal  $\theta$  obtained are validated by evaluating the objective using 1000 random samples. For example, the square box in Figure 6a shows the objective for the optimized Adam design evaluated using 1000



(a) Objective estimates (the square at the right end shows  $\hat{R}(\theta)$  for the optimal design from Adam evaluated using 1000 random samples)



(b) Constraint estimates

Fig. 6: Objectives and constraints for the non-failing methods with  $\lambda = 0$  for Example I.

random samples. Figure 7 shows the final designs associated with the non-failing methods.

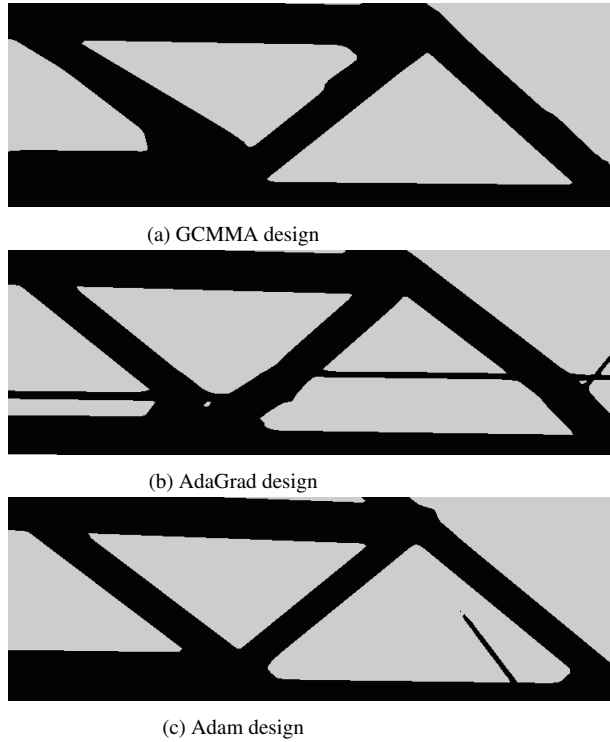


Fig. 7: Computed Designs for the non-failing methods with  $\lambda = 0$  for Example I.

In this example, Adadelata with an exponential decay rate  $\zeta = 0.95$  does not converge or converges very slowly as shown in Figure 8a. We can explain this behavior by considering the Algorithm 3 in Section 2, where we initialize  $\mathbf{a}_h$  and  $\mathbf{a}_\theta$  to zero. This, coupled with  $\rho$  close to 1.0 and small initial gradients, produce very small updates. We can use smaller values for  $\zeta$ , which results in Adadelata relying mostly on gradient values from previous iterations. However, significantly smaller  $\zeta$  does not alleviate this issue entirely.

The algorithms SAG and SVRG also fail to converge. The objective history of SAG and SVRG are shown in Figures 8b and 8c, respectively. Here, SAG is implemented with an ensemble size of  $N_s = 100$  and  $n = 4$  gradients are updated at every iteration. In TO, the design may go through large changes during the initial iterations. Hence, the failure of the algorithm is due to the significant use of gradient information from past iterations. For example, in SAG, only a handful of the gradients are updated at every iteration and most of the gradients from previous iterations are used. Updating many gradients (*i.e.*, large  $n$ ) at every iteration will produce converged results when using SAG as it will essentially become a full-batch gradient descent. However, this increases the overall computational cost of the optimization considerably compared to Adam and AdaGrad. We, therefore, do not pursue SAG any further in this work.

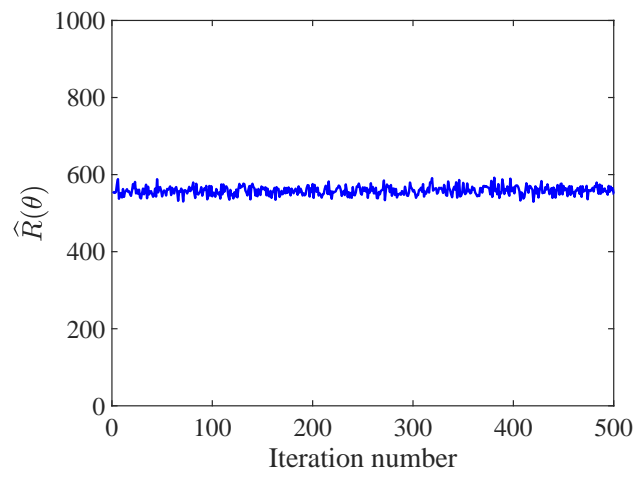
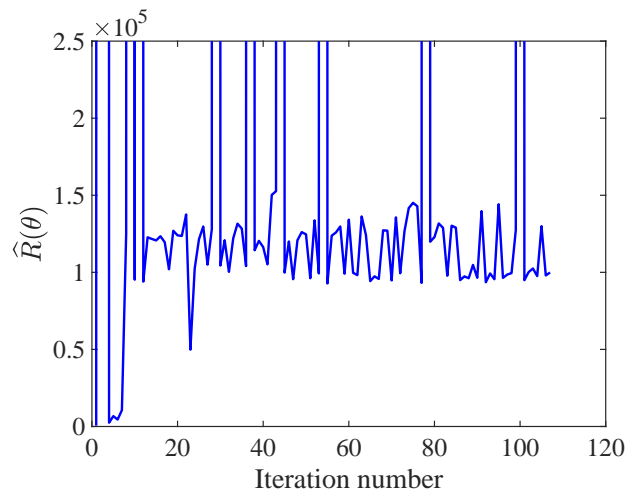
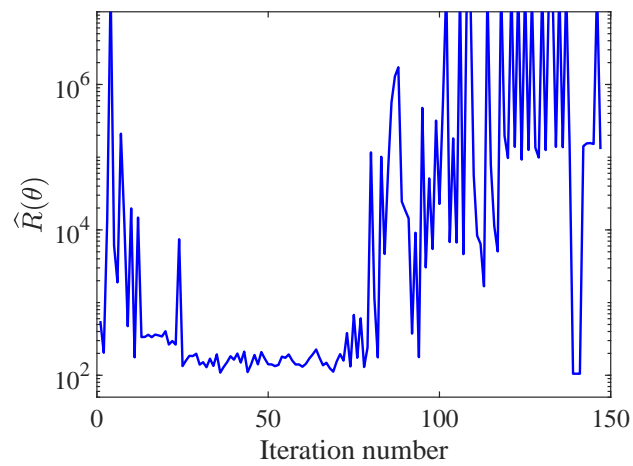
Similarly, in SVRG, gradients and parameter estimates from past iterations are maintained (see Algorithm 6). For example, in Figure 8c, SVRG with a small learning rate  $\eta = 0.005$  and a smaller number of inner iterations  $m = 4$ , *i.e.*, the  $\mathbf{h}_{\text{best}}$  can be from 4 latest iterations in past, shows the algorithm starts diverging when there is a significant change in the design (near iteration 75 in this case). For larger  $\eta$  and larger  $m$ , the algorithm diverges earlier. Even a smaller number of inner iterations,  $m$ , along with a much smaller learning rate,  $\eta$ , can be used, but this will increase the overall computational cost as  $\mathbf{h}_{\text{best}}$  will be evaluated more frequently as well as it will slow down the convergence. Hence, significant non-convexity of the objective function and heavy use of previous gradients cause SAG and SVRG algorithms to fail in this example.

Next, we use  $n = 50$  random samples per iteration and compare the objective for AdaGrad with our previous results obtained using  $n = 4$  random samples. Figure 9 shows that there is no noticeable improvement in the objective even though performing 50 forward solves per iteration is computationally expensive.

The success of the SGD methods (except Adadelta) depends on the choice of the learning rate  $\eta$ . Figure 10 shows results from AdaGrad with untuned and tuned  $\eta$ . Tuning  $\eta$  can be performed in a computationally inexpensive manner by performing only a few design optimization iterations with different  $\eta$  and selecting the most promising  $\eta$ . Furthermore, it is important to note that the success of these SGD methods for TO strongly depends on the use of an independent set of random samples  $\{\xi_i\}_{i=1}^n$  at every iteration. Figure 11 shows that if the same sample set  $\{\xi_i\}_{i=1}^4$  is used at every iteration the optimization method AdaGrad may get trapped in a local minimum similar to the untuned learning rate setting.

### 3.1.2 Robust Design

Next, we solve the optimization problem (8) subject to (9), for  $\lambda = 0.1$ . Here, we optimize a combination of mean and the variance of the objective subject to a similar combination of mean and variance of constraint values. Note that in this case the failures of some of the SGD methods are even more pronounced since the objective scales with the square of the compliance now. Again, we utilize a learning rate  $\eta = 0.05$  for the algorithms in Section 2 and a sample size of  $n = 4$ . Again, we confine the presentation of the results to algorithms that converge to more or less meaningful designs. For example, Adadelta, SVRG, and SAG fail to produce a meaningful design due to the reasons discussed before.

(a) Adadelta (with  $\zeta = 0.95$ )(b) SAG (with  $N = 100$  and  $n = 4$ )(c) SVRG (with  $N = 20$ ,  $m = 4$ , and  $\eta = 0.005$ )Fig. 8: Objectives for the failing methods with  $\lambda = 0$  for Example I.



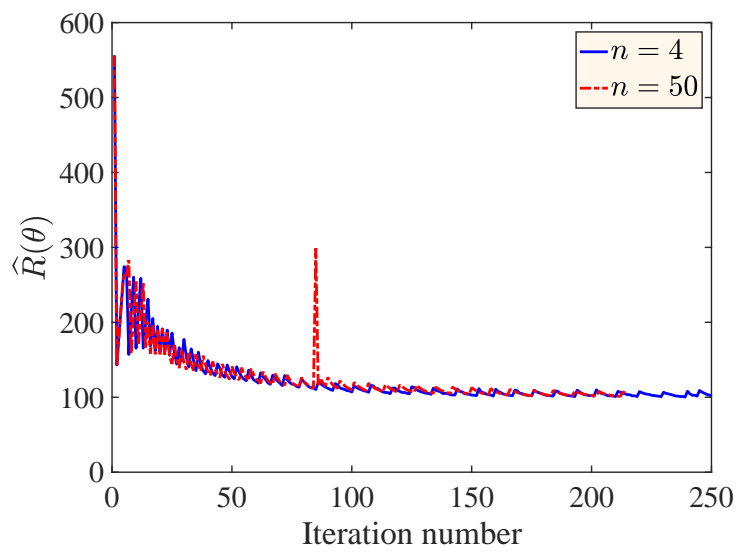


Fig. 9: Plot of objectives using AdaGrad with  $n = 4$  and  $n = 50$  samples per iteration with  $\lambda = 0$  for Example I.



(a) Untuned design



(b) Tuned design

Fig. 10: Tuning of learning rate  $\eta$  plays an important role in the success of the SGD methods. This figure shows final designs using AdaGrad without and with  $\eta$  tuned.

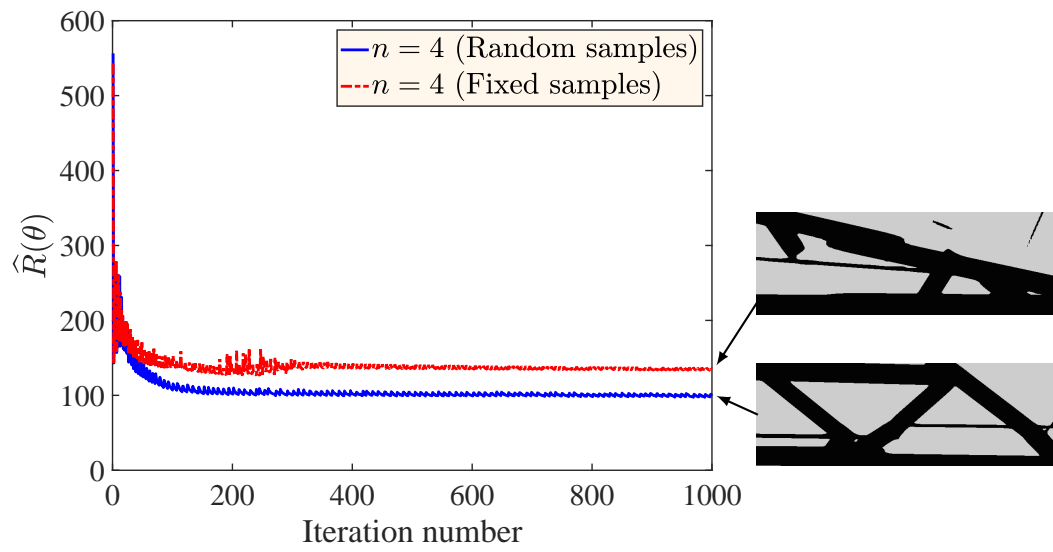


Fig. 11: Plot of objectives using AdaGrad with fixed and random samples per iteration with  $\lambda = 0$  for Example I.

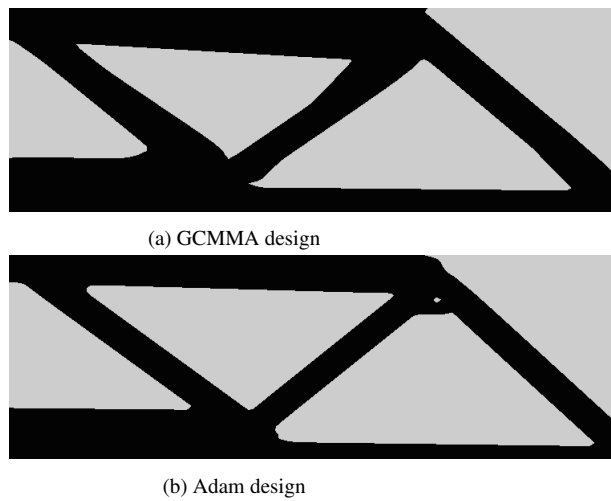
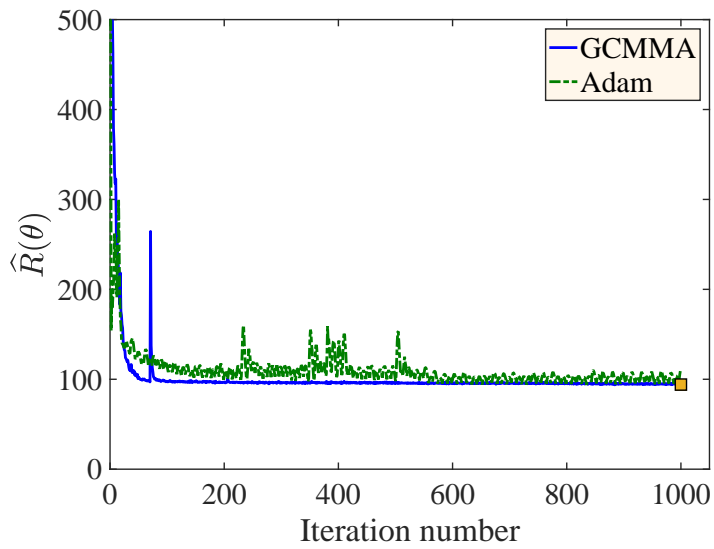
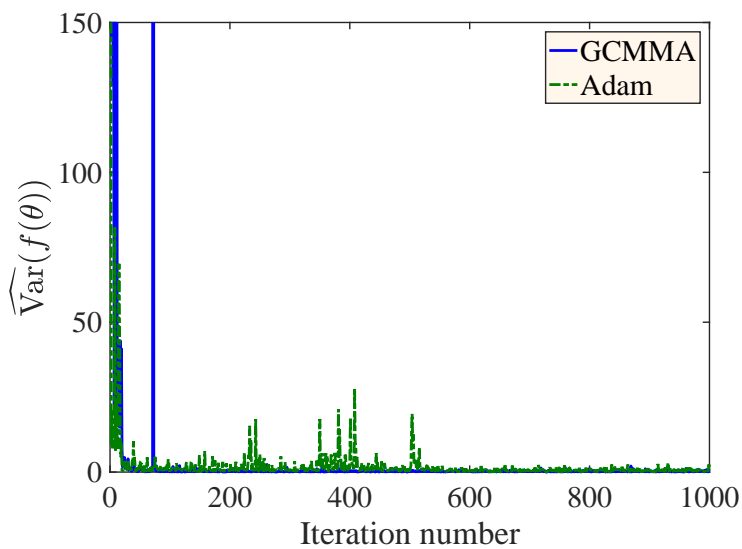


Fig. 12: Optimal robust designs for the non-failing methods with  $\lambda = 0.1$  for Example I.



(a) Objective estimates (the square at the right end shows  $\widehat{R}(\theta)$  for the optimal design from Adam evaluated using 1000 samples)



(b) Variance estimates

Fig. 13: Objectives and variances for the non-failing methods with  $\lambda = 0.1$  for Example I.

Here, the objective and constraint functions being optimized are not average values, but instead average plus 0.1 times the variance of those evaluated functions.

Among the SGD methods, only Adam maintains its stability while all other methods fail to converge to meaningful designs. Figure 12 shows the design produced by GCMMA and Adam. Figure 13 shows the objective function and the variance part of it for the designs constructed by GCMMA and Adam when using  $n = 4$  realizations of the uncertain inputs. The square at the right end in Figure 13a indicates the objective for the optimal design obtained from Adam using 1000 random samples.

To observe the effect of  $\lambda$  in the objective, next, we increase  $\lambda$  to 100. In Figure 14 we compare Adam and GCMMA for various mini-batch sizes. We run Adam with  $n = 4$ , which shows the convergence of the objective. However, GCMMA with  $n = 4$  and 10 does not converge. In Figure 14, we show the objective for GCMMA using  $n = 10$  with a solid blue line. We then increase  $n = 20$  for GCMMA and note that GCMMA converges (shown using the red dotted line in Figure 14). However, using  $n = 20$  random samples per iteration compared to 4 used for Adam is computationally expensive.

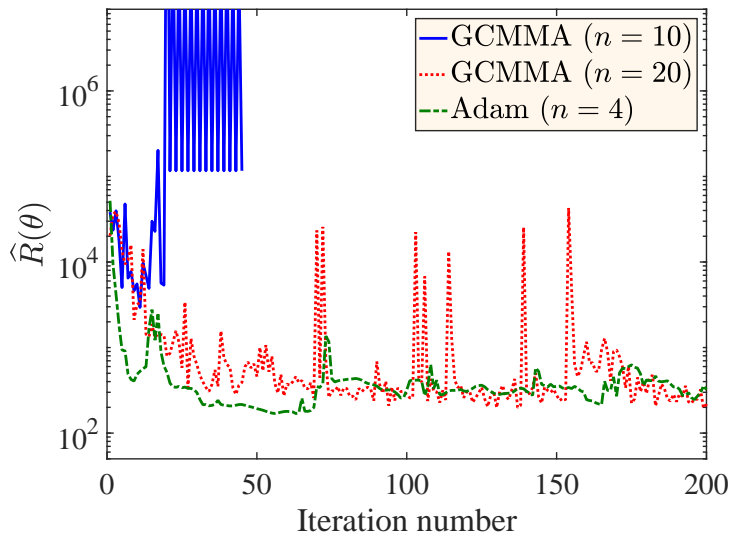


Fig. 14: Objective estimates with  $\lambda = 100$  for Example I.

This example uses a beam design problem under uncertainty to show the use of stochastic gradients for TO. We employ different stochastic gradient descent algorithms, namely, AdaGrad, Adadelta, Adam, SVRG, and SAG using only a handful of random samples per iteration. Among these algorithms, AdaGrad and Adam perform well after some tuning of their learning parameter and provides meaningful designs for  $\lambda = 0$  in the objective (see (8)). However, AdaGrad fails to provide a meaningful design when we increase  $\lambda$  to 0.1. GCMMA, which is typically not used for stochastic design problems, however, performs well and produces meaningful designs for  $\lambda = 0$  and  $\lambda = 0.1$ . Hence, among all the algorithms studied for this example, Adam

and GCMMA turn out to be the most useful to optimize the objective defined in (8). Note that, only first order gradients are used in all of these methods and hence their costs are comparable.

### 3.2 Example II: Load Support over Elastic Bedding

In the second example, we consider a 3D design problem with a structure being subject to uncertain loading and resting on an uncertain bedding. A design domain of size  $1.0 \times 1.0 \times 1.33$  rest on top of a non-design domain of size  $1.0 \times 1.0 \times 0.67$ ; see Figure 15. The non-design domain is occupied by a material with random stiffness and represents an uncertain bedding. The non-design domain is clamped at the bottom face. At the center of the top face of the design domain, a point load with random direction is applied. The performance measure of the objective function is the strain energy, and the only constraint is to ensure that the mass-ratio of the structure is no more than 15% of the maximum design mass, *i.e.*, the entire design-domain filled with bulk material. In this example, to enforce the constraint  $\kappa = 1000$  is used with the SGD methods.

In this example, the structural geometry is described by the combined density-level set method described in Section 2.1. In the first 200 optimization steps, we perform a standard SIMP optimization with  $\beta_{\text{SIMP}} = 3.0$ . To this end, we set the level set shift parameters to  $\phi_i = -10^{-3}$  and the density shift parameter to  $\theta_s = 10^{-3}$ . The final design of the SIMP optimization process is used to initiate a level set optimization process with a uniform bulk material in the solid domain. To this end we set, the level set shift parameters to  $\phi_i = 0.5$  and the density shift parameter to  $\theta_s = 1.0$ .

The random stiffness distribution in the non-design domain, *i.e.*, the Young's modulus  $E(\mathbf{x}, \boldsymbol{\xi})$ , is defined by the following tri-linear interpolation

$$E(\mathbf{x}, \boldsymbol{\xi}) = E_0 \sum_{i=1}^8 N_i(\mathbf{x}) \xi_i, \quad (43)$$

where  $E_0$  is a constant and assumed as unity,  $N_i$  are the tri-linear shape functions, and  $\xi_i$  the random variables associated with the Young's moduli at the corner points of the non-design domain. The random variables  $\xi_i$  are sampled from uniform distribution in  $(0, 1)$ . Uncertainty in the direction of the point load is described by two additional uniform random variables that define the direction cosines of the load vector as follows

$$\begin{aligned} \cos \gamma_x &= \sin(\pi \xi_9) \sin(2\pi \xi_{10}); \\ \cos \gamma_y &= \sin(\pi \xi_9) \cos(2\pi \xi_{10}); \\ \cos \gamma_z &= \cos(\pi \xi_9), \end{aligned} \quad (44)$$

where  $\gamma_x$ ,  $\gamma_y$ , and  $\gamma_z$  are the angles between the load vector and the  $x$ ,  $y$ , and  $z$  axes, respectively. In this example, we assume the Poisson's ratio as 0.3, the magnitude of the point load as unity, and fictitious springs with spring constant  $10^{-6}$  to avoid rigid body motion of disconnected material. The finite element model consists of tri-linear

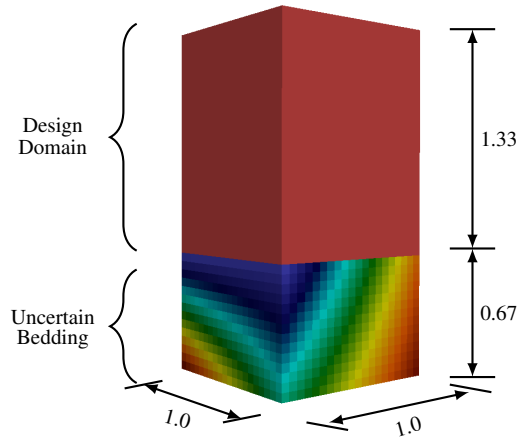


Fig. 15: Design area (top) and bedding (bottom) for Example II; the color contours show the Young's modulus distribution for specific realization of the uncertain bedding.

hexahedron elements with edge length as 0.05. This results in a mesh with 16,000 design parameters.

As the following numerical studies show, this optimization problem demonstrate key design differences that can arise from different stochastic gradient methods and GCMMA. We only use AdaGrad and Adam among the SGD methods in this example as they turned out to be more useful to TO problems under uncertainty as seen in the previous example. For illustration purposes, we present first results for the deterministic formulation of the optimization problem. Figure 16 shows optimized geometries for certain realizations of the random variables, highlighting the strong influence of the uncertain parameters on the design solutions.

### 3.2.1 Average Design

First, we consider solving the optimization problem (8) and (9), for  $\lambda = 0$ , *i.e.*, we do not account for the variance terms in the objective and constraint. We utilize a learning rate  $\eta = 0.35$  for the algorithms in Section 2 and a sample size of  $n = 4$ . The value for the learning rate was determined by a few preliminary runs. Figure 17 shows the evolution of the mean objective and constraint values.

Figure 18 shows the optimal designs obtained using the three methods. The final design obtained from all these three methods are quite different – GCMMA provides a four-legged; AdaGrad suggests a three-legged, and Adam delivers a one-legged design. However, when we compare the objectives from all these methods shown in Figure 17 we see that they are comparable and all of these are acceptable designs. When increasing the number of samples to  $n = 10$ , we notice that using more samples at each iteration does not improve the optimization significantly; see Figure 19 for Adam. We note that the same observation was made in Example I.

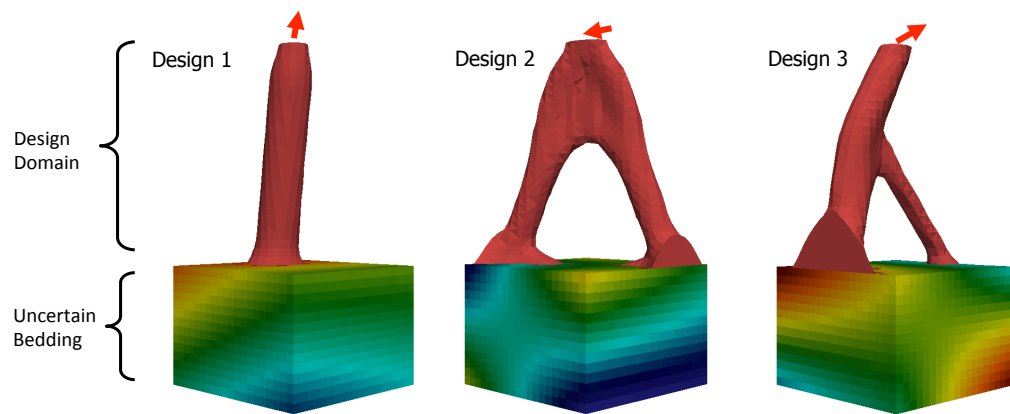
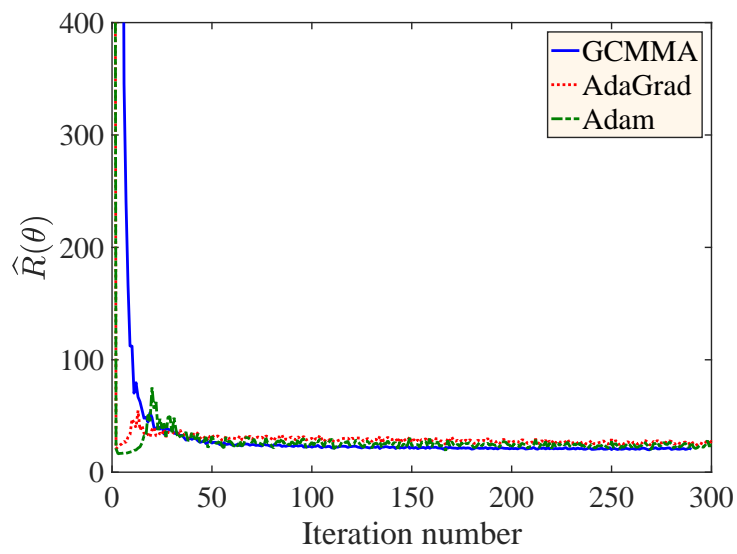
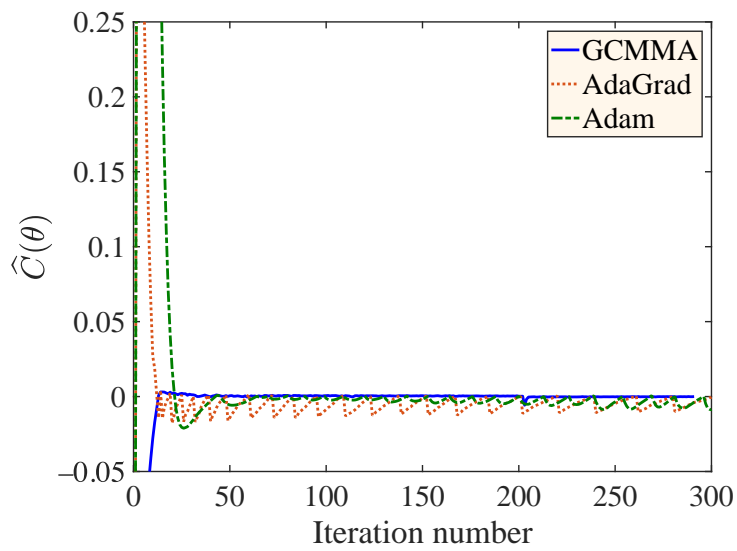


Fig. 16: Deterministic optimization results for three realizations of the random variables, namely, tri-linearly interpolated Young's modulus and direction of the load.



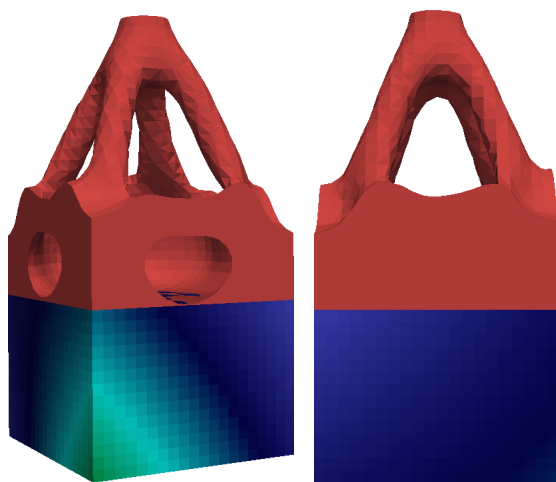
(a) Objective estimates



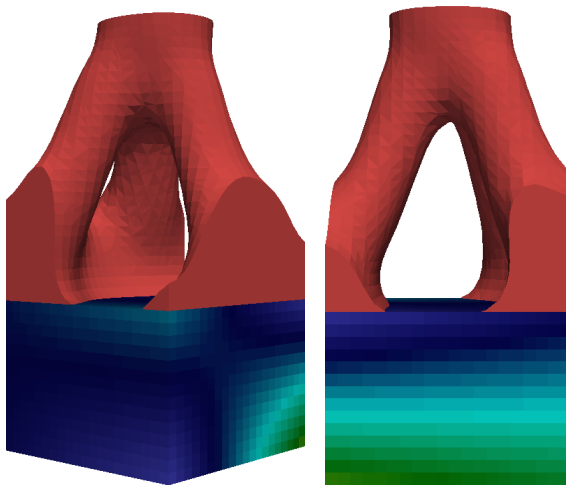
(b) Constraint estimates

Fig. 17: Objectives and constraints for three methods, namely, GCMMA, AdaGrad, and Adam with  $\lambda = 0$  for Example II.

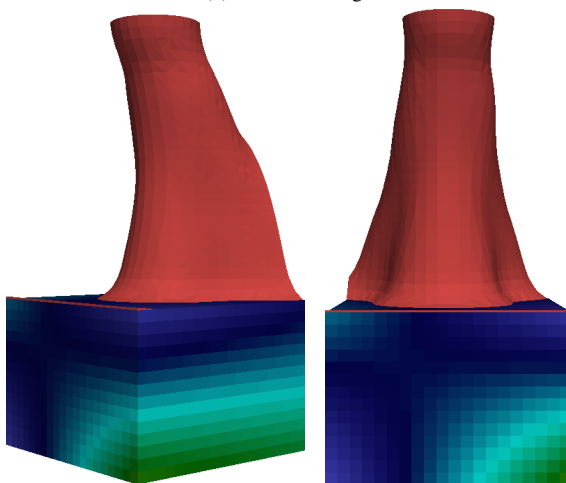




(a) GCMMA design



(b) AdaGrad design



(c) Adam design

Fig. 18: Computed designs for three methods, namely, GCMMA, AdaGrad, and Adam with  $\lambda = 0$  for Example II (side and front views are shown for each method, respectively).

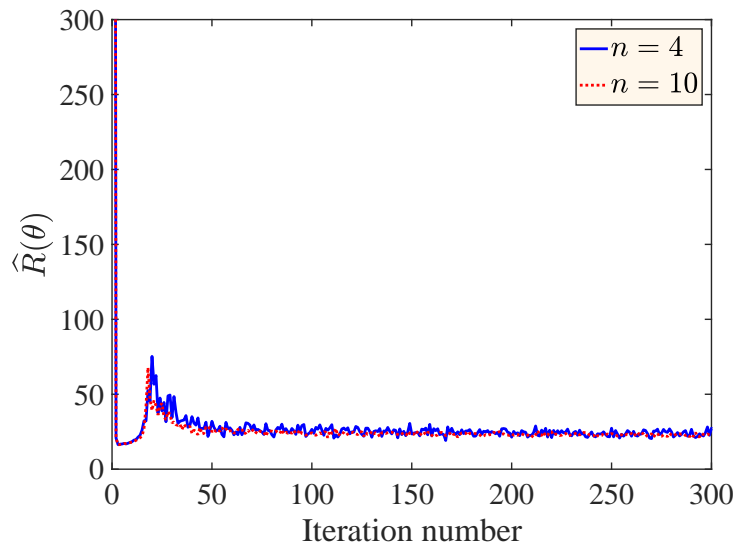


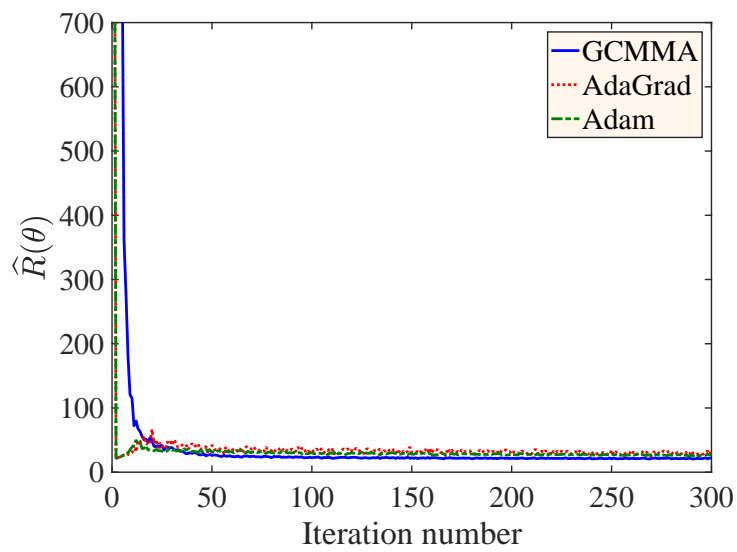
Fig. 19: Plot of objectives using Adam with  $n = 4$  and  $n = 10$  samples per iteration with  $\lambda = 0$  for Example II.

### 3.2.2 Robust Design

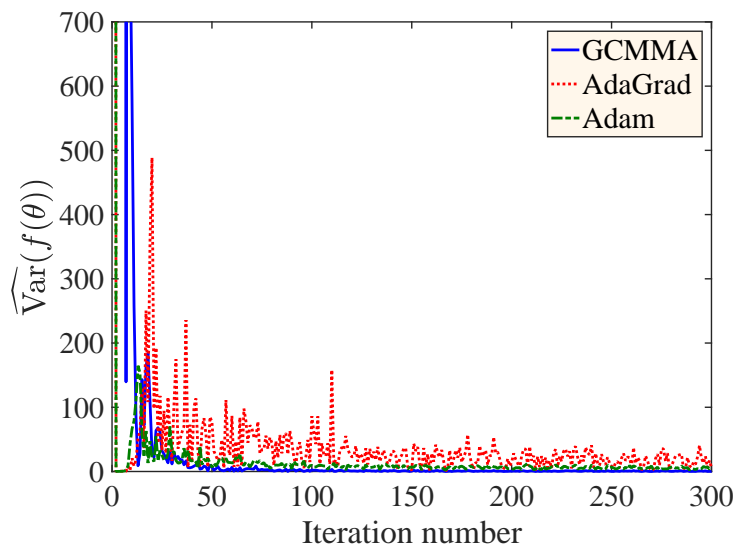
Here, we consider solving the optimization problem (8) subject to (9), for  $\lambda = 0.01$ , *i.e.*, we seek to optimize a combination of mean and the variance of the objective subject to a similar combination of mean and variance of constraint values. We again utilize a learning rate parameter  $\eta = 0.35$  for the algorithms in Section 2.3 and a sample size of  $n = 4$ .

Figure 20 shows the evolution of the objective  $\widehat{R}(\boldsymbol{\theta})$  and variance  $\widehat{\text{Var}}(f(\boldsymbol{\theta}))$  for designs determined by GCMMA, AdaGrad, and Adam. The two SGD methods show rapid decrease in the objective  $\widehat{R}(\boldsymbol{\theta})$  and variance  $\widehat{\text{Var}}(f(\boldsymbol{\theta}))$  in the first few iterations. Figure 20b indicates that the proposed use of stochastic gradients for TOuU is useful to produce a robust design with a smaller variance of  $f(\boldsymbol{\theta})$ . Figure 21 shows the final designs obtained using the three methods. While GCMMA provides a four-legged design as before, AdaGrad and Adam provide one-legged designs. However, if we compare their objectives, we can see that they are comparable. Hence, all of these are acceptable optimal designs. Among the stochastic gradient descent methods, however, Adam outperforms AdaGrad for minimizing the variance as shown in Figure 20(b).

In this example, Adam and GCMMA perform well in the presence of uncertainty even though final designs obtained from them are different. AdaGrad, in this example, produces meaningful designs for  $\lambda = 0$  as well as for  $\lambda = 0.01$ . However, in terms of robustness of the design AdaGrad design is inferior to the Adam and GCMMA designs as seen in Figure 20, which shows larger variance for the AdaGrad design. The reason behind Adam outperforming AdaGrad is due to the fact that Adam accumulates both gradients and squared gradient information over the iteration and uses these two accumulated quantities in the update. This stabilizes the design update even when the gradients are large. On the other hand, AdaGrad only accumulates the squared gradient information for updating the designs.

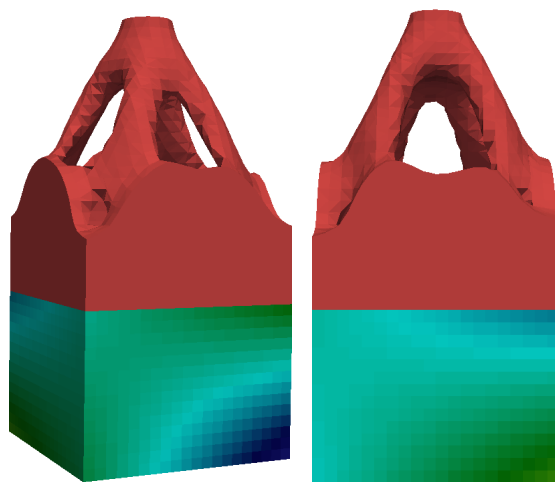


(a) Objective estimates

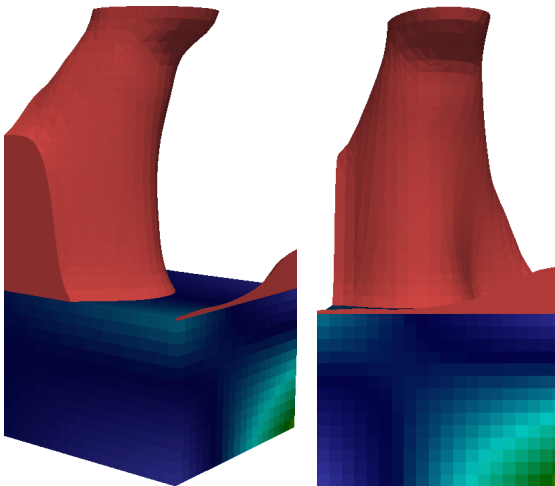


(b) Variance estimates

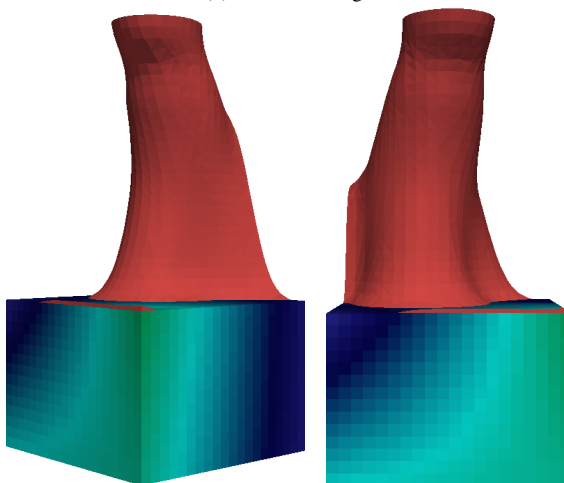
Fig. 20: Objectives and variances for the three methods used with  $\lambda = 0.01$  for Example II.



(a) GCMMA design



(b) AdaGrad design



(c) Adam design

Fig. 21: Computed designs for three methods, namely, GCMMA, AdaGrad, and Adam with  $\lambda = 0.01$  for Example II (side and front views are shown for each method, respectively).

## 4 Conclusions

Topology optimization under high-dimensional uncertainty that utilizes gradient-based approaches requires multiple evaluations of the objective, constraints, and the gradients. This incurs a significant computational cost and often becomes practically infeasible. In this paper, we reduce this computational cost of TOuU by using a stochastic approximation of the gradients. These approximations are calculated with only a few random samples per iteration (*e.g.*,  $n = 4$  in the numerical examples). This approach helps us reduce the cost of TOuU to only a modest multiple of deterministic TO. To implement our proposed approach, we employ some of the SGD methods popular in machine learning domain while supplying them with stochastic gradients. We also use GCMMA, an optimizer with history in TO for our numerical examples while supplying stochastic gradients to it. The first TOuU problem, a highly non-convex beam design problem, shows that while GCMMA can often perform well, it requires fair estimates of the gradients for large  $\lambda$ . Among five SGD methods employed here, AdaGrad and Adam perform well in this example. The damping of gradients in AdaGrad and Adam helps to navigate the design space. In the second TO problem, a load is supported over an uncertain elastic bedding with uncertain loading direction. In this example, GCMMA, AdaGrad, and Adam again produce acceptable designs with comparable objectives. Both of these examples show that the use of stochastic gradients estimated with a small number of random samples at each iteration produces meaningful designs in a computationally inexpensive manner. Further, the optimized structure obtained using SGD methods has objective values similar to GCMMA for topology optimization under uncertainty.

## 5 Acknowledgements

The authors acknowledge the support of the Defense Advanced Research Projects Agency (DARPA) TRADES project. Computations for the results presented in Section 3 are performed on Lonestar5, a high-performance computing resource operated by the Texas Advanced Computing Center (TACC) at University of Texas, Austin.

## References

- Alvarez, F. and Carrasco, M. (2005). Minimization of the expected compliance as an alternative approach to multiload truss optimization. *Structural and Multidisciplinary Optimization*, 29(6):470–476.
- Asadpoure, A., Tootkaboni, M., and Guest, J. K. (2011). Robust topology optimization of structures with uncertainties in stiffness – Application to truss structures. *Computers & Structures*, 89(11-12):1131–1141.
- Bae, K.-r. and Wang, S. (2002). Reliability-based topology optimization. In *9th AIAA/ISSMO Symposium on Multidisciplinary Analysis and Optimization*, page 5542.
- Bendsøe, M. P. (1989). Optimal shape design as a material distribution problem. *Structural Optimization*, 1(4):193–202.

- Blatman, G. and Sudret, B. (2010). An adaptive algorithm to build up sparse polynomial chaos expansions for stochastic finite element analysis. *Probabilistic Engineering Mechanics*, 25(2):183–197.
- Bottou, L. (2010). Large-scale machine learning with stochastic gradient descent. In *Proceedings of COMPSTAT'2010*, pages 177–186. Springer.
- Bottou, L. (2012). Stochastic gradient descent tricks. In *Neural networks: Tricks of the trade*, pages 421–436. Springer.
- Bottou, L., Curtis, F. E., and Nocedal, J. (2018). Optimization methods for large-scale machine learning. *SIAM Review*, 60(2):223–311.
- Burger, M., Hackl, B., and Ring, W. (2004). Incorporating topological derivatives into level set methods. *Journal of Computational Physics*, 194(1):344–362.
- Burman, E. and Hansbo, P. (2014). Fictitious domain methods using cut elements: III. A stabilized nitsche method for stokes problem. *ESAIM: Mathematical Modelling and Numerical Analysis*, 48(3):859–874.
- Chen, S. and Chen, W. (2011). A new level-set based approach to shape and topology optimization under geometric uncertainty. *Structural and Multidisciplinary Optimization*, 44(1):1–18.
- Chen, S., Chen, W., and Lee, S. (2010). Level set based robust shape and topology optimization under random field uncertainties. *Structural and Multidisciplinary Optimization*, 41(4):507–524.
- Collins, M. D. and Kohli, P. (2014). Memory bounded deep convolutional networks. *arXiv preprint arXiv:1412.1442*.
- Conti, S., Held, H., Pach, M., Rumpf, M., and Schultz, R. (2009). Shape optimization under uncertainty: a stochastic programming perspective. *SIAM Journal on Optimization*, 19(4):1610–1632.
- Deaton, J. D. and Grandhi, R. V. (2014). A survey of structural and multidisciplinary continuum topology optimization: post 2000. *Structural and Multidisciplinary Optimization*, 49(1):1–38.
- Doostan, A. and Owhadi, H. (2011). A non-adapted sparse approximation of pdes with stochastic inputs. *Journal of Computational Physics*, 230(8):3015–3034.
- Doostan, A., Owhadi, H., Lashgari, A., and Iaccarino, G. (2009). Non-adapted sparse approximation of PDEs with stochastic inputs. Technical Report Annual Research Brief, Center for Turbulence Research, Stanford University.
- Duchi, J., Hazan, E., and Singer, Y. (2011). Adaptive subgradient methods for on-line learning and stochastic optimization. *Journal of Machine Learning Research*, 12(Jul):2121–2159.
- Dunning, P. D. and Kim, H. A. (2013). Robust topology optimization: minimization of expected and variance of compliance. *AIAA Journal*, 51(11):2656–2664.
- Dunning, P. D., Kim, H. A., and Mullineux, G. (2011). Introducing loading uncertainty in topology optimization. *AIAA Journal*, 49(4):760–768.
- Eldred, M. S. and Elman, H. C. (2011). Design under uncertainty employing stochastic expansion methods. *International Journal for Uncertainty Quantification*, 1(2).
- Eom, Y.-S., Yoo, K.-S., Park, J.-Y., and Han, S.-Y. (2011). Reliability-based topology optimization using a standard response surface method for three-dimensional structures. *Structural and Multidisciplinary Optimization*, 43(2):287–295.

- Ghanem, R. G. and Spanos, P. D. (2003). *Stochastic Finite Elements: A Spectral Approach*. Dover publications.
- Guest, J. K. and Igusa, T. (2008). Structural optimization under uncertain loads and nodal locations. *Computer Methods in Applied Mechanics and Engineering*, 198(1):116–124.
- Guo, X., Zhang, W., and Zhong, W. (2014). Doing topology optimization explicitly and geometrically – a new moving morphable components based framework. *Journal of Applied Mechanics*, 81(8):081009–081009–12.
- Haldar, A. and Mahadevan, S. (2000). *Probability, Reliability, and Statistical Methods in Engineering Design*. Wiley New York, 1st edition.
- Hampton, J. and Doostan, A. (2016). Compressive sampling methods for sparse polynomial chaos expansions. *Handbook of Uncertainty Quantification*, pages 1–29.
- Jansen, M., Lombaert, G., and Schevenels, M. (2015). Robust topology optimization of structures with imperfect geometry based on geometric nonlinear analysis. *Computer Methods in Applied Mechanics and Engineering*, 285:452–467.
- Johnson, R. and Zhang, T. (2013). Accelerating stochastic gradient descent using predictive variance reduction. In *Advances in Neural Information Processing Systems*, pages 315–323.
- Jung, H.-S. and Cho, S. (2004). Reliability-based topology optimization of geometrically nonlinear structures with loading and material uncertainties. *Finite Elements in Analysis and Design*, 41(3):311–331.
- Keshavarzzadeh, V., Fernandez, F., and Tortorelli, D. A. (2017). Topology optimization under uncertainty via non-intrusive polynomial chaos expansion. *Computer Methods in Applied Mechanics and Engineering*, 318:120–147.
- Keshavarzzadeh, V., Meidani, H., and Tortorelli, D. A. (2016). Gradient based design optimization under uncertainty via stochastic expansion methods. *Computer Methods in Applied Mechanics and Engineering*, 306:47–76.
- Kharmanda, G., Olhoff, N., Mohamed, A., and Lemaire, M. (2004). Reliability-based topology optimization. *Structural and Multidisciplinary Optimization*, 26(5):295–307.
- Kim, C., Wang, S., Rae, K.-r., Moon, H., and Choi, K. K. (2006). Reliability-based topology optimization with uncertainties. *Journal of Mechanical Science and Technology*, 20(4):494.
- Kingma, D. and Ba, J. (2014). Adam: A method for stochastic optimization. *arXiv preprint arXiv:1412.6980*.
- Kreissl, S. and Maute, K. (2012). Levelset based fluid topology optimization using the extended finite element method. *Structural and Multidisciplinary Optimization*, 46(3):311–326.
- Lavergne, T., Cappé, O., and Yvon, F. (2010). Practical very large scale CRFs. In *Proceedings of the 48th Annual Meeting of the Association for Computational Linguistics*, pages 504–513. Association for Computational Linguistics.
- Lazarov, B. S., Schevenels, M., and Sigmund, O. (2012). Topology optimization considering material and geometric uncertainties using stochastic collocation methods. *Structural and Multidisciplinary Optimization*, 46(4):597–612.



- Liu, C., Zhu, Y., Sun, Z., Li, D., Du, Z., Zhang, W., and Guo, X. (2018). An efficient moving morphable component (MMC)-based approach for multi-resolution topology optimization. *arXiv preprint arXiv:1805.02008*.
- Mahsereci, M. and Hennig, P. (2015). Probabilistic line searches for stochastic optimization. In *Advances in Neural Information Processing Systems*, pages 181–189.
- Martin, M., Krumscheid, S., and Nobile, F. (2018). Analysis of stochastic gradient methods for PDE-constrained optimal control problems with uncertain parameters. Technical report, Institute of Mathematics, École Polytechnique Fédérale de Lausanne.
- Maute, K. (2014). Topology optimization under uncertainty. In *Topology Optimization in Structural and Continuum Mechanics*, pages 457–471. Springer.
- Maute, K. and Frangopol, D. M. (2003). Reliability-based design of mems mechanisms by topology optimization. *Computers & Structures*, 81(8-11):813–824.
- Maute, K., Weickum, G., and Eldred, M. (2009). A reduced-order stochastic finite element approach for design optimization under uncertainty. *Structural Safety*, 31(6):450–459.
- Mogami, K., Nishiwaki, S., Izui, K., Yoshimura, M., and Kogiso, N. (2006). Reliability-based structural optimization of frame structures for multiple failure criteria using topology optimization techniques. *Structural and Multidisciplinary Optimization*, 32(4):299–311.
- Moon, H., Kim, C., and Wang, S. (2004). Reliability-based topology optimization of thermal systems considering convection heat transfer. In *10th AIAA/ISSMO Multidisciplinary Analysis and Optimization Conference*, page 4410.
- Norato, J.A. and Bell, B. and Tortorelli, D. (2015). A geometry projection method for continuum based topology optimization with discrete elements. *Computer Methods in Applied Mechanics and Engineering*, 293:306–327.
- Novotny, A., Feijó, o, R., Taroco, E., and Padra, C. (2003). Topological sensitivity analysis. *Computer Methods in Applied Mechanics and Engineering*, 192(7-8):803–829.
- Novotny, A., Feijó, o, R., Taroco, E., and Padra, C. (2007). Topological sensitivity analysis for three-dimensional linear elasticity problem. *Computer methods in applied mechanics and engineering*, 196(41-44):4354–4364.
- Ross, S. M. (2013). *Simulation*. Academic Press, 5th edition.
- Roux, N. L., Schmidt, M., and Bach, F. R. (2012). A stochastic gradient method with an exponential convergence rate for finite training sets. In *Advances in Neural Information Processing Systems*, pages 2663–2671.
- Ruder, S. (2016). An overview of gradient descent optimization algorithms. *arXiv preprint arXiv:1609.04747*.
- Schott, B., Rasthofer, U., Gravemeier, V., and Wall, W. (2014). A face-oriented stabilized nitsche-type extended variational multiscale method for incompressible two-phase flow. *International Journal for Numerical Methods in Engineering*.
- Schuëller, G. I. and Jensen, H. A. (2008). Computational methods in optimization considering uncertainties – an overview. *Computer Methods in Applied Mechanics and Engineering*, 198(1):2–13.
- Sharma, A., Villanueva, H., and Maute, K. (2017). On shape sensitivities with Heaviside-enriched XFEM. *Structural and Multidisciplinary Optimization*,

- 55(2):385–408.
- Sigmund, O. and Maute, K. (2013). Topology optimization approaches: A comparative review. *Structural and Multidisciplinary Optimization*, 48(6):1031–1055.
- Sigmund, O. and Petersson, J. (1998). Numerical instabilities in topology optimization: A survey on procedures dealing with checkerboards, mesh-dependencies and local minima. *Structural Optimization*, 16(1):68–75.
- Sutskever, I., Martens, J., Dahl, G., and Hinton, G. (2013). On the importance of initialization and momentum in deep learning. In *International Conference on Machine Learning*, pages 1139–1147.
- Svanberg, K. (1987). The method of moving asymptotes – a new method for structural optimization. *International Journal for Numerical Methods in Engineering*, 24(2):359–373.
- Tootkaboni, M., Asadpoure, A., and Guest, J. K. (2012). Topology optimization of continuum structures under uncertainty – A Polynomial Chaos approach. *Computer Methods in Applied Mechanics and Engineering*, 201:263–275.
- Tsuruoka, Y., Tsujii, J., and Ananiadou, S. (2009). Stochastic gradient descent training for L1-regularized log-linear models with cumulative penalty. In *Proceedings of the Joint Conference of the 47th Annual Meeting of the ACL and the 4th International Joint Conference on Natural Language Processing of the AFNLP: Volume 1*, pages 477–485. Association for Computational Linguistics.
- Villanueva, C. H. and Maute, K. (2014). Density and level set-XFEM schemes for topology optimization of 3-D structures. *Comput. Mech.*, 54(1):133–150.
- Zeiler, M. D. (2012). Adadelta: an adaptive learning rate method. *arXiv preprint arXiv:1212.5701*.
- Zhang, W. and Kang, Z. (2017). Robust shape and topology optimization considering geometric uncertainties with stochastic level set perturbation. *International Journal for Numerical Methods in Engineering*, 110(1):31–56.
- Zhang, W., Yuan, J., Zhang, J., and Guo, X. (2016). A new topology optimization approach based on moving morphable components (MMC) and the ersatz material model. *Structural and Multidisciplinary Optimization*, 53(6):1243–1260.
- Zhao, J. and Wang, C. (2014). Robust topology optimization of structures under loading uncertainty. *AIAA journal*, 52(2):398–407.
- Zhou, M. and Rozvany, G. (1991). The COC algorithm, Part II: Topological, geometrical and generalized shape optimization”. *Computer Methods in Applied Mechanics and Engineering*, 89(1):309 – 336.